UNIVERSITÄT OSNABRÜCK

Structure and Functional Dynamics of the KdpFABC P-type ATPase from *Escherichia coli*

D i s s e r t a t i o n

zur Erlangung des Grades eines

Doctor rerum naturalium
(Dr. rer. nat)

eingereicht am Fachbereich Biologie / Chemie
der Universität Osnabrück

von

Thomas Heitkamp

Osnabrück, Februar 2009

Ein Gelehrter in seinem Laboratorium ist nicht nur ein Techniker;

er steht auch vor den Naturgesetzen wie ein Kind vor der Märchenwelt.

Marie Curie

PREFACE

The results are presented in three chapters. Chapter 1 has already been published (Heitkamp *et al.*, 2008) and chapter 2 is a submitted manuscript. The last chapter is currently in preparation for publication. These three chapters represent the results of this study, which provides new insights into the structure of the KdpFABC complex from *Escherichia coli* and into the functional dynamics of P-type ATPases in general.

ACKNOWLEDGMENT

No one acts alone. This thesis would not have been possible without the contributions of a large number of individuals.

In particular, I would like to express my deep gratitude to my supervisor Prof. Dr. Karlheinz Altendorf, who made my Ph.D. thesis possible by providing excellent material, financial and scientific support. Furthermore, I want to thank for the possibility to work autonomously but never alone.

I am grateful to Prof. Dr. Robert Tampé for the evaluation of this thesis.

I am highly indebted and grateful to the mentor of my research carrier, Dr. Jörg-Christian Greie for the excellent aid and guidance during my Ph.D. thesis. He showed me to hold the line, when everything seemed to go wrong. Special thanks also go to Jörg for the friendly atmosphere in the lab and the unlimited patience, when I was slow off the mark once again.

I want to thank my collaboration partners in Stuttgart, namely Dr. Michael Börsch and Nawid Zarrabi for introducing me in the field of single molecule ALEX-FRET. Their great interest for this strange P-type ATPase and the extensive discussions about the, sometimes more or less confusing, data renders this work possible. In particular, I am grateful to Nawid, who spent a lot of time for generating the Hidden-Markov-Models. Beside the scientific aspects, I always felt like a member of your group, especially during the soccer world championship (Italy-Germany 0:2). And I also learned some vocabulary of a strange language ("Ja allerhopp!").

I also would like to thank Dr. Bettina Böttcher and her group for the introduction into the technique of TEM and single particle analysis. When the situation seemed hopeless, she had always some ideas.

I want to thank all members of the Arbeitsgruppe Mikrobiologie for the familiar atmosphere and the cooperativeness in scientific and private problems. In this way I would like to acknowledge Thomas ("Der Grieche"), Knut and Inga for sharing with me the fermentation job and all members of the "Party lab community". Your friendship made this time for one of the best times in my life.

A very special thank goes to the 119 lab community, namely Doris, Dorthe, Ertan, Henrik, Jörg, René ("Der Kanalreiniger"), Sabrina, Stefan ("Zwiebel"), Thomas ("Der Grieche") and Ulla for all the small things, which made the work in the lab to a pleasure. Especially, I want to thank Henrik and Dorthe for the intensive discussions and their open ear also for private problems.

All work is not possible without good friends. I would like to mention my closest friend Timo. I never want to miss our discussions about the secrets in chemistry, horror films, science fiction and the power of Uri Geller ("Besenkammer").

In special, I want to express my deepest thank to my parents and my brothers, who were at my side during my whole life. Their everlasting love and help represent an indestructible anchor in sometimes complicated and frustrating times.

Finally, I deeply thank Kerstin for her undivided support and patience with a sometimes extremely confused guy. I will always be grateful for her love.

TABLE OF CONTENTS

Chapter III

Conformational Dynamics of the KdpFABC P-type ATPase from
Escherichia coli **Revealed by Single Molecule ALEX-FRET**

Abbreviations

A-domain	actuator domain
ADP	adenosine-5'-diphosphate
ALEX	alternating laser excitation
AMP	adenosine-5'-monophosphate
AMP-PNP	adenosine 5'-(β, γ-imido)triphosphate
Ap^R	ampicilline resistance
ATP	adenosine-5'-triphosphate
ATPase	adenosine triphosphatase
BSA	bovine serum albumine
DiSC3(5)	3,3'-dipropylthiadicarbocyanin-jodide
DTT	dithiothreitole
ECL	enhanced chemiluminescence
EDTA	ethylenediaminetetraacetic acid
FPLC	„fast protein liquid chromatography"
FRET	fluorescence resonance energy transfer
HMM	Hidden-Markov-Model
HRP	horseradish peroxidase
IgG	immuneglobuline G
KdpBN	isolated, recombinant nucleotide-binding domain of KdpB, including deca-histidinyl tag
$KdpC_{90-188}$	C-terminal part of KdpC (residues 90-188)
$KdpC_{sol}$	soluble part of KdpC (residues 39-190)
K_M	Michaelis-Menten constant
MES	2-(N-morpholino)-ethanesulfonic acid
MPM	membrane/P-loop/membrane
N-domain	nucleotide binding domain
NEM	N-ethylmaleimide
NMR	nuclear magnetic resonance
NTA	nitrilotriacetic acid
OCS	oligocyclic suboxides
OD_x	optical density at a certain wavelength x
P-domain	phosphorylation domain
PAGE	polyacrylamide-gelelectrophorese
PCR	polymerase chain reaction

P_i	ortho-phosphat (inorganic phosphate)
PMSF	phenyl-methylsulphonyl fluoride
SDS	sodium dodecylsulfate
SERCA	Ca^{2+}-ATPase of sarco(endo)plasmic reticulum
TCEP	tris-(2-carboxyethyl)-phosphine
TEM	transmission electron microscopy
TM	transmembrane helix
TM-domain	transmembrane domain
Tris	tris-(hydroxymethyl)-aminomethane
UV	ultraviolet light
v/v	volume per volume
V_{max}	maximal reaction velocity of enzyme catalyzed reactions
w/v	weight per volume

GENERAL INTRODUCTION

Ion gradients and potassium transporting proteins in Bacteria

The accumulation of potassium ions (K^+) within the cytoplasm and the exclusion of sodium ions (Na^+) is a major attribute of every living cell ([1, 2]). The potassium ions are primarily used for the generation of turgor pressure. In addition, cytoplasmic K^+ plays a role in the activation of enzymes ([3]) and in pH homeostasis (For overview: [4]), whereby the regulation of cytoplasmic pH is a sum effect of the K^+,H^+-antiporter ([5]) and the Na^+,H^+-antiporter ([6]). These ion fluxes are carried out and regulated by a variety of membrane proteins including ion channels, transporters and proteins in response to environmental conditions.

One of the most important stress factor in bacteria is connected to the osmolality of the surrounding medium. Due to fast fluctuations in osmolality, the prokaryotic cell needs a fast response system. As a first response to an osmotic upshock, a massive K^+ accumulation in the cytoplasm can be observed in order to avoid extreme water efflux, which rises the concentration of K^+ from 200-500 mM under normal conditions up to the molar range. The K^+ influx is mainly achieved by activation of the Trk potassium uptake systems ([7]). Simultaneously, the bacteria synthesize organic anions like glutamate ([8, 9]), which serve as a counterbalance for the positively charged potassium ions. As a secondary response when the K^+ concentration reaches a critical point, the cells synthesize or take up so-called compatible solutes, which can either be zwitterionic like proline, glycine betaine or ectoine ([7, 10-12]), or they can be uncharged carbohydrates like trehalose ([13, 14]). In the case of a fast decrease of medium osmolality (osmotic downshock) bacteria counteract with a complete loss of potassium glutamate and trehalose ([15]). Due to these different reactions upon a change in medium osmolality, the *E. coli* cell requires a set of specialized potassium transport systems (Figure 1).

The homologous potassium channels KefB and KefC ([16]) are mainly responsible for K^+-efflux. In addition, they are essential for the detoxification of electrophile reagents like methylglyoxal or NEM ([17]). Beside the Kef systems, a so far biochemically uncharacterized K^+/H^+-antiporter also plays a role in potassium efflux ([18]). In the case of a rather drastic decrease of external osmolality, K^+ ions leave the cytoplasm together with other small molecules by means of mechanosensitive channels. Electrophysical data led to the notion that there are three types of mechanosensitive channels according to their different opening behaviour over a membrane pressure gradient ([19]).

At external K^+ concentrations above 200 µM, K^+ is taken up by the constitutively expressed TrkG/TrkH and Kup systems. The Trk systems exhibit moderate affinities for potassium (K_M: 0.3-1 and 2.2-3 mM, respectively) but high uptake rates (v_{max}: 240 µmol g^{-1} min^{-1} and 310-450 µmol g^{-1} min^{-1}, respectively) ([20]). This transport system is built up of at least three

subunits. The membrane-integral subunit TrkG or TrkH transports the ion into the cytoplasm (*4*). The TrkA protein is capable of binding NAD(H), whereas the membrane-associated Sap protein binds ATP. However, although the transport depends on both the proton motive force and ATP, the ATP is merely needed for activation and is not hydrolyzed (*21*)

The Kup system doesn't seem to play a role in osmoadaptation (*15*). It transports potassium with rather low affinity as well as low uptake rates (K_M: 0.3 mM; v_{max}: 30 µmol g^{-1} min^{-1}) (*22*) and, in contrast to the other potassium uptake systems, it lacks the discrimination between K$^+$ and Rb$^+$ and also transports Cs$^+$. Similar to the Trk systems, the K$^+$ transport seems to be driven by a H$^+$ symport (*4*)
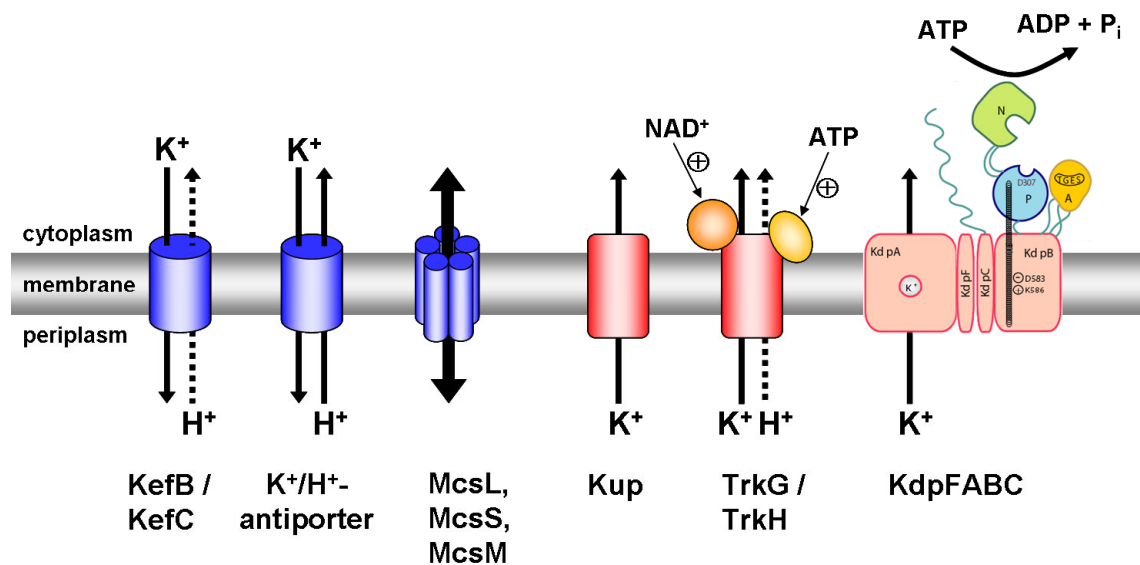
Figure 1: Schematic overview of K$^+$-transporting systems in *Escherichia coli*. According to ref *23* with changes described in ref *4*, *24* and *25*.

Regulation of Kdp expression

When the K$^+$ concentration in the medium falls below 100 µM, the constitutively expressed low affinity K$^+$ uptake systems (Trk, Kup) are no longer sufficient to meet the cell's demand for potassium. Therefore, under these conditions many prokaryotes express a high affinity K$^+$ uptake system, the KdpFABC complex (*26, 27*). The coupling of ion transport to ATP hydrolysis leads to a very high potassium affinity (K_M: 2 µM) but only to moderate transport rates (v_{max}: 150 µmol g^{-1} min^{-1}) (*28*).

The Kdp system is genetically organized in a regulon, which consist of two adjacent operons (Figure 2). The first operon is built up of four structural genes, which are coding for the membrane-integrated KdpFABC complex (*26, 29, 30*). The regulation of this operon is mediated by the gene products of the second operon (*31, 32*). The membrane-bound sensor kinase KdpD and the cytoplasmic response regulator KdpE belong to the family of two-component sensor

kinase/response regulator systems (*33*). KdpD is inserted into the membrane by a bundle of four transmembrane helices. The N-terminal and C-terminal part of the protein is oriented toward the cytoplasm (*34*).
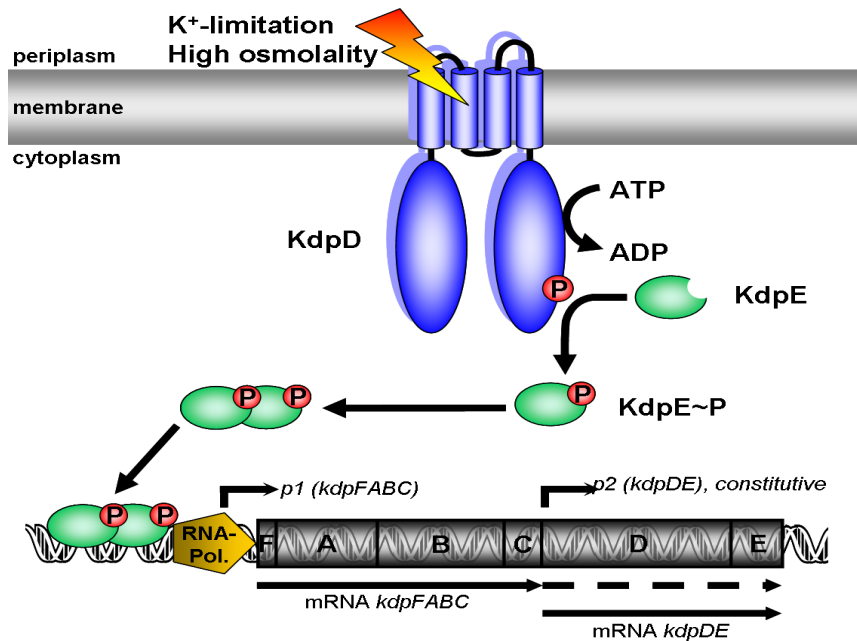

Figure 2: Organization and Regulation of the *kdpFABCDE* regulon.

Upon sensing a so far controversially discussed stimulus, dimerized KdpD undergoes ATP-mediated autophosphorylation at the conserved histidine residue 673 in the C-terminal part of the protein (*35, 36*). The phosphoryl group is then transferred to the conserved aspartate 52 of the response regulator KdpE (*35, 37*), which thereupon also dimerises. Dimeric KdpE-P finally binds to the promoter region of the *kdpFABC* operon and induces its transcription as a classical helix-turn-helix transcription factor (*37*). If there is no stimulus, non-phosphorylated KdpD is also able to dephosphorylate KdpE-P, which leads to a termination of KdpFABC synthesis (*38*).

The KdpFABC complex – a P-type ATPase

The KdpFABC complex belongs to the superfamily of P-type ATPases, a family of homologous enzymes of both eukaryotic and prokaryotic origin. All members of these family comprise the formation of an acid-stable and alkali-labile phosphointermediate (*39*). They function as primary ion pumps, generally transporting cations across membranes by use of the free Gibbs energy provided by the phosphorylation, resulting in the formation and maintenance of large ion gradients (*40*). All P-type ATPases share some common structural features. The catalytic subunit can be structurally divided into four domains, each of which comprising specific functions. In the case of

the KdpFABC complex, only the KdpB subunit exhibits all these structural domains (*41*) (see also Figure 1 of Chapter 2). Furthermore, the KdpFABC complex comprises three additional subunits, which have no counterparts in other P-type ATPases: KdpA, which shares similarities to K^+-channels from the KcsA-type and mediates K^+ transport, KdpC, which seems to play a role in ATP binding, and KdpF, which probably acts as a molecular glue (*42*). These four subunits form the KdpFABC complex in a 1:1:1:1 stoichiometry (*42*). Based on kinetic data, the KdpFABC complex seems to exhibit two catalytically active ATP binding sides. However, the structure of the nucleotide binding domain (N-domain) of KdpB as well as the comparison with other P-type ATPases renders the presence of two ATP-binding sides within one KdpB subunit unfavorable (*43*). Therefore, the KdpFABC complex most likely exhibits an at least dimeric state like many other P-type ATPases. The functional state of the Na^+,K^+-ATPase is most likely a tetramer (*44*). For the H^+-ATPase from *Neurospora crassa*, an active oligomeric ring-like structure as well as an active monomeric state has been shown (*45, 46*). However, experimental data regarding the oligomeric state of the KdpFABC complex is still lacking. Hence, the first chapter of this thesis deals with the analysis of the oligomeric state of the KdpFABC complex via several biochemical and biophysical approaches.

The KdpB subunit

As already mentioned, only the KdpB subunit (72 kDa) comprises the typical four common functional and structural domains of P-type ATPases: The transmembrane domain, the phosphorylation domain, the actuator domain and the nucleotide binding domain (*41*).

The transmembrane domain: The transmembrane domain (TM-domain) anchors the protein into the membrane. According to the transport specificity and to the origin of the particular P-type ATPase, P-type ATPases span the membrane seven to ten times. The KdpB subunit of the KdpFABC complex most likely exhibits seven transmembrane helices as predicted by extensive sequence comparison (*47*). These transmembrane helices also most likely reflect the core motif of the TM-domain of every P-type ATPase known so far (*48*). The heavy metal-transporting ATPases exhibit up to nine transmembrane helices due to N-terminal extensions carrying the large cytoplasmic heavy metal binding cluster. Many other mainly eukaryotic P-type ATPases are anchored to the membrane by ten transmembrane helices, with the additional three helices extending at the C-terminus. In general, the TM-domain carries the ion binding sites. Only the KdpFABC complex, in which ion binding and transport is mediated by a separate subunit, is an exception (*41*). However, in this case of KdpFABC, the TM-domain is involved in coupling ATP hydrolysis to ion transport. Instead of a conserved ion binding site, two residues, namely D583 and K586, which are located in the center of transmembrane helix five (TM5), are conserved among all

KdpB polypeptides sequenced so far (*49*). Substitutions of these residues resulting in the elimination of the corresponding charge readily lead to a more or less severe uncoupling of ATP hydrolysis and K^+ transport (*49*). Therefore, these charged residues seem to play an essential role for functional coupling.

The actuator domain: The actuator domain (A-domain) is connected to the transmembrane domain by short linker sequences. The structure of the A-domain of the sarcoplasmic reticulum Ca^{2+}-ATPase (SERCA) exhibits ten β-strands together with two α-helices (*50*). A conserved TGE motif can be found in the A-domain of almost all P-type ATPases. Most likely, this motif plays a role in the dephosphorylation of the E2-P catalytic state of P-type ATPases (*40, 51*). Furthermore, during the catalytic cycle (see below) the TGE motif is supposed to approach the phosphorylation site in the E2-P and E2 states of the enzyme. In SERCA, mutation of any residue within the TGE motif hindered the E1~P $\leftrightarrow$ E2-P transition resulting in a non-functional enzyme, thereby indicating a mediating function of the A-domain in the communication between the ATP and the calcium binding sites (*52*).

The phosphorylation domain: The phosphorylation domain (P-domain) resembles the most conserved module among P-type ATPases and carries the conserved DKTGT motif (*48*). The mere presence of this key motif classifies a protein to the superfamily of P-type ATPases. This motif contains the asparte residue, D307 in KdpB, which is reversibly phosphorylated by the γ-phosphoryl group of ATP. Due to its core structure, the P-domain belongs to a large group of enzymes named according to the L-2-haloacid dehalogenase, the HAD superfamily (*53*). All P-domains comprise the same secondary structural elements with six- or seven-stranded parallel β-sheets flanked by short α-helices forming a typical Rossman fold (*50, 54*). As already mentioned, the aspartate residue forms the characteristic transient acylphosphate. The typical P-type ATPase inhibitor *ortho*-vanadate most likely seems to bind near the aspartate, thereby sterically preventing the formation of an acylphosphate (*50*). Other conserved residues within the P-domain are involved in the coordination of Mg^{2+}, which, in turn, is needed to stabilize the γ-phosphate group of the ATP molecule during hydrolysis. The P-domain is also structurally linked to the transmembrane domain, whereby one transmembrane helix (TM5 in most cases) extends through the membrane into the P-domain and ends right underneath the phosphorylation site. It was shown for SERCA, that the P-domain changes its internal structure and orientation with respect to TM5 upon binding of the γ-phosphate of ATP together with Mg^{2+} (*55*), which results in a rearrangement of the ion binding sides within the transmembrane domain. In the case of KdpB, the orientation of the conserved charged residues in TM5 towards the neighboring KdpA subunits is supposed to be altered by a similar mechanism, which could exert an effect on the K^+ bound by KdpA (*40*). However, despite these internal structural changes the orientation of the P-domain within KdpB most likely remains the same during catalysis.

The nucleotide binding domain: Due to its solubility and its folding properties, the structure of the nucleotide binding domain (N-domain) of many P-type ATPases has been solved by either NMR spectroscopy or by X-ray crystallography. The N-domain of SERCA has been solved in several conformational states via crystallography (*50, 55-60*). The structure of the Na$^+$,K$^+$-ATPase N-domain has been solved by NMR (*61*) and also by crystallography (*62*). Furthermore, the cytoplasmatic loop including the N- and P-domains of the copper-transporting P-type ATPase CopA from *Archeoglobus fulgidus* has been solved by crystallization (*54*). The solution structures of the N-domains of the eukaryotic Wilson disease protein (WDP) (*63*) and of the bacterial KdpB subunit (*43, 65*) have also been solved by NMR. This set of solution structures from N-domains of different P-type ATPases offered the ability to compare the nucleotide binding mechanism of P-type ATPases in detail.

The N-domain is linked to the P-domain via two flexible loops. Although especially the N-domains of eukaryotic P-type ATPases comprise rather large insertions, their core structure is basically the same. This core structure is resembled by the N-domain of KdpB (KdpBN), which is the smallest representative known so far (*65*). KdpBN is composed of a curved, six-stranded anti-parallel β-sheet domain, which is flanked by two α-helices on one side (*43, 64*). Evolutionary progress from bacterial to eukaryotic P-type ATPases most likely led to the insertion of additional sequences into this minimal structure due to the necessity of more complex regulatory circuits (*65*). These insertions could interact with accessory proteins, which, therefore, could be responsible for altered nucleotide binding affinities in eukaryotic P-type ATPases (*66-68*).

With the growing number of N-domain structures available it becomes apparent that despite of the same core structure, the particular mode of nucleotide binding differs among P-type ATPases. However, in all cases the nucleotide is oriented within a binding pocket in a way that the γ-phosphate protrudes out of the pocket and, thus, faces the conserved aspartate residue in the P-domain. Furthermore, most P-type ATPases like SERCA or KdpB exhibit a conserved KGXX(D/E) motif. The conserved lysine residue together with a phenylalanine located 20-25 amino acids towards the N-terminus were shown to be crucial for nucleotide binding (*69-70*).

In order to analyze the particular ATP-binding mode of KdpBN, the solution structure of KdpBN was solved by NMR both in the absence of a nucleotide (apo-form) and with bound AMP-PNP (holo-form). The results revealed that the ATP-binding mode comprises similarities to SERCA but also some unique features (Figure 3) (*43, 71*). The contacts between the N-domain and the nucleotide were shown to be limited to only a few residues. As in almost all P-type ATPases (For overview: *72*), a conserved phenylalanine residue, F377 in KdpB, interacts with the aromatic rings of the bound ATP by means of stacking of their π-electron systems. In contrast to SERCA, the conserved lysine residue K395 of the KGXX(D/E) motif interacts with the purine ring system of the nucleotide by a cation-π-stacking mode. In KdpB, the phosphate groups of the ATP are

flanked by the two arginine residues R317 and R382, which is corresponding to SERCA with its counterparts in R489 and R560. The NMR spectroscopy-derived structures of KdpBN show only slight differences between the apo- and the holo-form indicating a preformed nucleotide binding pocket, in which the nucleotide is merely clipped in an almost linear conformation, which facilitates the release of the γ-phosphate to the neighboring P-domain (*43*). The major consequence of this proposed ATP-binding mode of KdpBN is the rather high binding constant for ATP, i.e. 1.4 mM (*43*), which is in strong contrast to other P-type ATPases. The N-domain of SERCA comprises a K_d for ATP in the range of 10-100 µM (*73*), which is similar to that of the Wilson disease protein N-domain with 70 µM, although the latter is more closely related to KdpB than SERCA (*63*). This discrepancy, especially with respect to the Wilson disease protein N-domain structure, most likely results from the fact that KdpBN comprises no interactions with the ribose moiety of the bound ATP molecule (*43*), whereas in the Wilson disease protein, the ribose is well coordinated within a proper ribose binding pocket (*63*). With respect to this discrepancy, a mechanism has been suggested, in which the KdpC subunit acts as a catalytical chaperone for a cooperative ATP binding (see below).
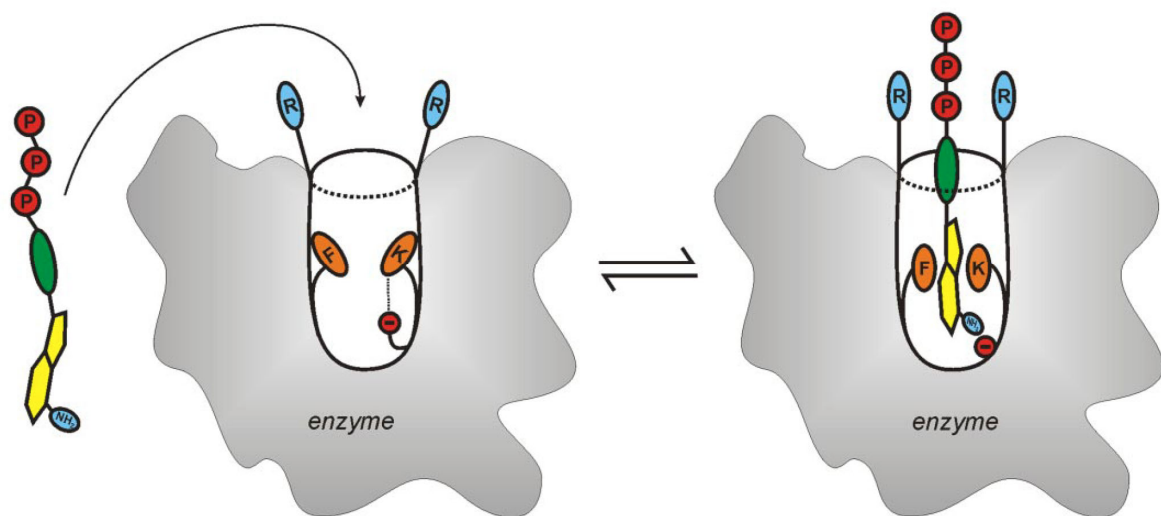
Figure 3: The nucleotide binding pocket of the N-domain of KdpB. The schematic drawing of the nucleotide binding pocket illustrates the rather simple nucleotide binding mode, enabling the rapid nucleotide exchange necessary for a functional reaction cycle. Highlighted are the residues F377, K395, R317 and R382. D344 is depicted as a negative charge at the *bottom* of the binding pocket by a *red circle* (*43*)

The KdpA subunit

Although KdpB comprises the typical features of P-type ATPases, the lack of ion binding sites within the catalytical subunit distinguishes the KdpFABC complex from all other representatives of this superfamily (*48*). In fact, the translocation of potassium is mediated by a single subunit, KdpA (59 kDa), which has no corresponding counterpart or domain element in other P-type ATPases

(*74-77*). The reduction of the transmembrane domain of KdpB to only seven transmembrane helices reflects this unique mechanism of ion translocation among P-type ATPases. The KdpA subunit shows strong similarities to potassium channels from the KcsA-type, which has initially been demonstrated by comparative computational sequence analysis of potentially related proteins (*78*). Whereas KcsA from *Streptococcus lividans* is built up of four identical polypeptides each with one MPM-motif (membrane/P-loop/membrane) (*79*), KdpA comprises four MPM-motifs within one polypeptide, which are flanked by two additional transmembrane helices. These findings led to the notion, that KdpA is evolutionary derived from a homotetrameric K$^+$-channel of the MPM-type by gene duplication and fusion events (*78*). Experimental evidence supporting this hypothesis came from already existing data on mutations affecting the K$^+$-selectivity and from the analysis of the transmembrane topology (*75, 78*). Additionally, the resulting model has successfully been used as a template for the identification and characterization of the corresponding ion selectivity filter regions within KdpA (*74, 77*). In these studies, mutations affecting ion selectivity were found to cluster within four distinct hydrophilic regions, each which is flanked by one transmembrane helix on either side. Another KcsA-derived structural model of KdpA based on a corresponding pairwise alignment of the four MPM-motifs together with the connecting loop regions also clearly demonstrated the clustering of these mutations in properly assembled pore regions (*41*). Despite the similarities of KdpA to potassium channels of the KcsA-type, K$^+$ gating and transport have to differ from K$^+$-channels. Whereas KcsA enables a passive diffusion of potassium ions across membranes, the KdpFABC complex is able to generate an over 10,000-fold gradient by active transport. Therefore, the KdpA subunit has to be tightly sealed from the cytoplasmatic side in order to prevent potassium backflow. Furthermore, the ion transport against the concentration is energized by the ATP hydrolysis in KdpB. As described above, the conserved dipole residues in TM5 of KdpB seem to play a crucial role in functional coupling of the two subunits. However, the distance between these residues and the potassium binding side in KdpA is too large for direct electrostatic interactions. Hence, there have to be other residues within the KdpA subunit in order to further transmit coupling events. In this respect, the two additional helices of KdpA, which don't comprise any homology to K$^+$-channels, as well as arginine 493, which is located in the C-terminal helix of the endmost MPM-motif, eventually play an essential role in energy coupling. In this context it is noteworthy that mutagenesis of this residue was shown to result in a complete loss of function of the KdpFABC complex (*80*).

The KdpC subunit

The function of the third subunit of the KdpFABC complex, namely KdpC (21 kDa), is still not yet fully understood. Earlier experiments showed that KdpC is essential for the function of the

KdpFABC complex (*81*). Nevertheless, the polypeptide comprises no homologies to any other protein known so far. KdpC consists of only one N-terminal transmembrane helix followed by a large cytoplasmic extension (*81*). For some time, this subunit was regarded as a member of the FXYD protein family like phospholamban or calmodulin as in the case of SERCA (*66*) or like the γ-subunit of the Na$^+$,K$^+$-ATPase (*68*), which all regulate protein activity via interactions with the large cytoplasmic loops of the catalytic subunit. However, none of these enzymes proved to be essential for protein activity, which led to the notion that KdpC exhibits a more unique function. The distinct function of the KdpC subunit became much clearer when it was found that the hydrophilic portion of KdpC (KdpC$_{sol}$) was able to bind one ATP molecule to a well-defined binding site within its C-terminal part (*82*). This KdpC domain could reach the catalytic domains of KdpB, which led to the notion that KdpC might exert a regulatory function by binding of ATP directly or in interaction with the nucleotide binding pocket of KdpB. The experiments further demonstrated that KdpC binds the ATP with a rather high binding constant in the millimolar range, i. e. weak binding, which was explained by the fact that only the ribose moiety of ATP is supposed to interact with KdpC$_{sol}$ (*82*). These findings resulted in a new model of cooperative ATP binding by KdpC and KdpB. As already described, the isolated N-domain of KdpB (KdpBN) also exhibits a rather untypical low binding affinity for ATP (K$_d$: 1.4 mM), which is most likely due to lacking interactions with the ribose moiety of the nucleotide. These findings suggest that KdpC acts as a catalytical chaperone by binding the ATP via the ribose moiety, thereby orienting and/or locking the nucleotide into the nucleotide binding pocket of KdpB (*41*).

The KdpF subunit

The KdpF subunit (3 kDa) is one of the smallest proteins known so far and comprises only one transmembrane helix with no further extensions. Nevertheless, it is an important component of the KdpFABC complex. Although the deletion of KdpF has no effect on the activity of the complex *in vivo*, purification of resulting KdpABC complexes resulted in an enzyme preparation with a complete loss in ATPase activity, combined with a high tendency of the complex to disintegrate (*83*). However, the addition of purified KdpF or simply *E. coli* lipids restored ATPase activity, which indicates that this hydrophobic subunit acts as a lipid-like stabilizer of the complex (*83*).

Subunit arrangement within the KdpFABC complex

Although there is yet some information about the structure and function of the single subunits within KdpFABC, only rudimentary data is available about their functional arrangement within the

complex. Electron microscopic or tomographic low resolution structures of KdpFABC arranged in 2D crystal lattices only solved the cytoplasmic domains of the complex, thereby lacking any information on the large membrane fraction of the enzyme (*84, 85*). However, structural information on also the membrane portion of the complex is of fundamental importance for the understanding of the interplay between the subunits. Especially the elucidation of the energy coupling mechanism between KdpB and KdpA as well as the cooperative ATP binding mechanism of KdpB and KdpC would clearly benefit from structural information on the arrangement of the corresponding transmembrane domains. In this thesis, the solution structure of the entire KdpFABC complex was solved by single particle analysis of negatively stained electron microscopic images (Chapter 2), thereby providing new insights in subunit arrangement and also resolving the transmembrane fraction of the enzyme.

The putative reaction cycle of the KdpFABC complex

All P-type ATPases share a widely accepted reaction scheme, which became prominent under the name "Albers-Post mechanism" (*86, 87*). The characteristic feature of this reaction cycle is the alternating presence of two distinct states, called E1 and E2, each of which comprising different structural as well as biochemical properties (*40*). In the transition between these two states, large domain movements occur, whereby the most drastic one is the N-domain swinging back and forth toward the P-domain (*50, 55*). Furthermore, the A-domain is supposed to rotate to some extend along its long axis, which results in an alteration of the orientation of the conserved TGES motif with respect to the P-domain (*50, 55*). The P- and the TM-domains undergo rather minor structural alterations in order to couple the energy of ATP hydrolysis/(de-)phosphorylation to ion transport. The putative reaction cycle of the KdpFABC complex according to ref *41* is shown in Figure 4.

In the E2 state of the complex, KdpA is supposed to exhibit a high affinity for potassium ions on the extracellular side of the membrane. Due to its low binding constant, ATP is in rapid exchange with the flexibly hinged N-domain (movement indicated by arrows). The absence of a distinct ATP-induced conformational change in the N-domain supported the idea that the N-domain is flexibly linked to the P-domain and engages or disengages the P-domain merely by thermal Brownian fluctuations (*43, 65*). The binding of potassium ions within KdpA probably triggers the rearrangement of the transmembrane helices of KdpB, which is depicted by the stretching of transmembrane helix five, thus converting the complex into the E1 state with an increased affinity for ATP. This increase is eventually mediated by a movement of the cytosolic part of KdpC toward the ATP binding pocket of the KdpB N-domain, which is explained by the cooperative ATP binding of the N-domain and KdpC. In this state, the N-domain is, however, supposed to retain its

flexibility, which allows swinging back and forth for the unlikely case that no cytoplasmic ATP is present.
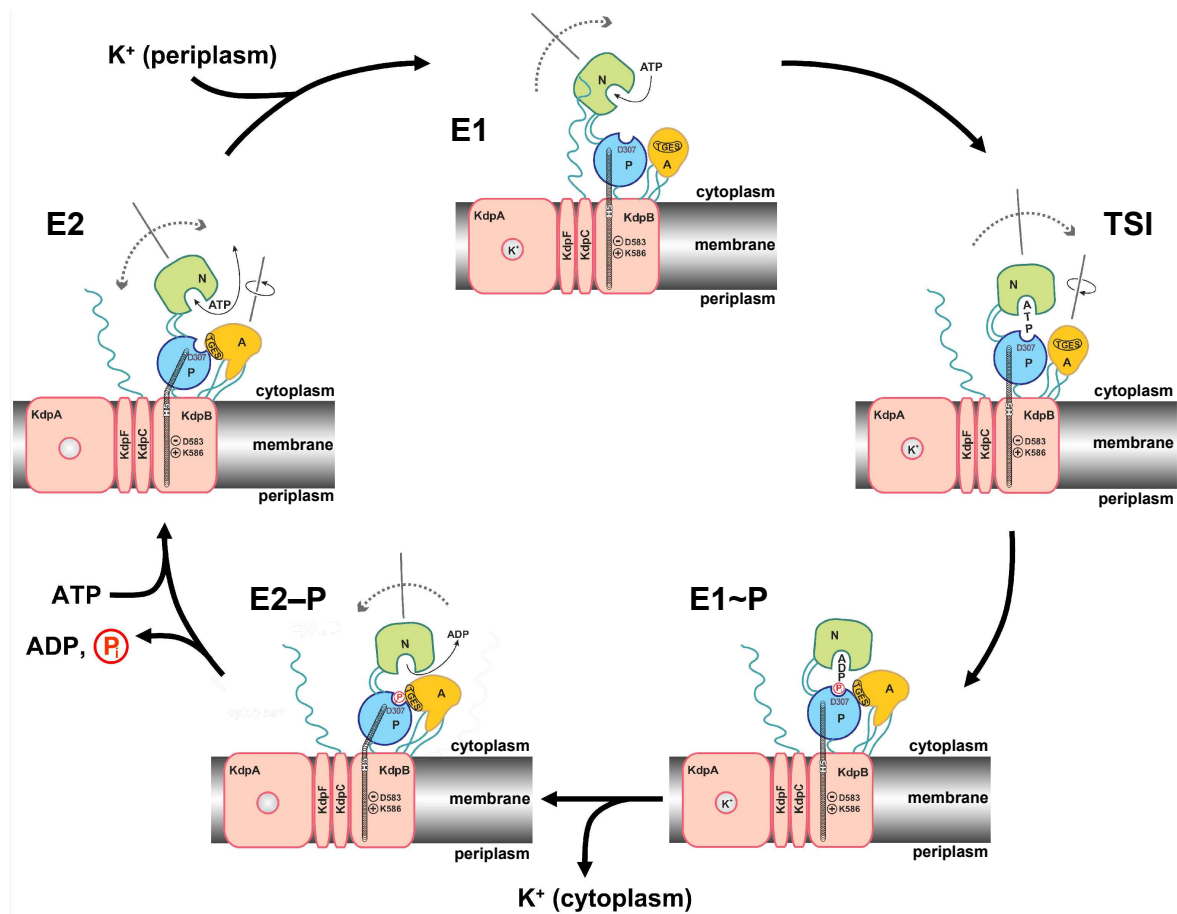
Figure 4: Proposed reaction cycle of the KdpFABC complex. Binding of a potassium ion to the E2 state of the enzyme promotes high affinity ATP binding within the N-domain of KdpB, which is probably mediated by KdpC. Subsequently, the KdpFABC complex is transformed to its E1 state, and the potassium ion is able to enter the binding site within KdpA. Upon entering the transition state (TSI) followed by phosphorylation, the potassium ion becomes occluded. The subsequent E1/E2 transition, which is accompanied by major conformational rearrangements in KdpB, alters the orientation of the dipole formed by D583 and K586 in the transmembrane domain of KdpB, which finally results in pushing the ion toward the cytoplasmic side of the membrane, where it is released. Dephosphorylation of the complex regenerates the E2 state. According to ref *41*.

Upon ATP binding, the N-domain moves toward the P-domain, which results in the trapping of the nucleotide between the N-domain and residue D307 of the P-domain, thereby rendering the cooperative interaction with KdpC dispensable. This transition state (TSI) has been introduced into the Post-Albers-scheme in order to describe this rather complex domain interaction pattern. Although there is yet no experimental evidence on the position of the A-domain within the transition state, it presumably rotates its TGES motif toward the P-domain as indicated by the circular arrow. Nucleotide binding and subsequent activation of the γ-phosphate group leads to the high energy E1~P state. Subsequently, the formation of the phosphoenzyme causes a conformational change within the transmembrane region (E2-P state), which alters the orientation

of the dipole formed by D583 and K586 in the transmembrane helix five of KdpB. This somehow renders the position of the potassium ion in KdpA energetically unfavorable and, as a consequence, pushes the ion toward the cytoplasmic side of the membrane, where it is subsequently released. Finally, the ADP molecule, which still bridges the N- and the P-domains, is released by a backswing of the N-domain, which enables the nucleotide to diffuse out of its binding pocket. The E2 state is then regenerated by the dephosphorylation of D307 via the TGES motif of the A-domain.

Although the current view on putative domain motions during the catalytic cycle of P-type ATPases is rather detailed, these conclusions merely result from the interpretation of indirect data like crystallization of inactive or inhibited protein conformations representing substeps within the reaction cycle, from the modulation of the intrinsic tryptophan fluorescence or from proteolytic digestion experiments (For overview: *72, 88-91*). Therefore, direct conclusions regarding the dynamics and transitions of and between the conformational states, especially with respect to dwell times and flexibility, are rather rare. In order to solve this eminent problem in the understanding of the P-type ATPase reaction mechanism, single molecule fluorescence resonance energy transfer (FRET) using the alternating laser excitation (ALEX) of reconstituted and catalytically active KdpFABC complexes was measured in this thesis (Chapter 3). For the first time, these experiments bridge over the cleft between crystal structures and real time protein dynamics in the field of P-type ATPases.

REFERENCES

1. Harold, F. M., and Altendorf, K. (1974) Cation transport in bacteria: K^+, Na^+ and H^+. *Curr. Top. Membr. Transp. 5*, 1-50.

2. Bakker, E. P. (1993) Cell K^+ and K^+ transport systems in prokaryotes. In: *Alkali cation transport systems in prokaryotes* (Bakker, E.P., ed.), pp. 205-224, CRC Press, Boca Raton, Florida.

3. Suelter, C. H. (1970) Enzymes activated by monovalent cations. Patterns and predictions for these enzyme catalysed reactions are explored. *Science 168*, 789-795.

4. Stumpe, S., Schlösser, A., Schleyer, M., and Bakker, E. P. (1996) K^+ circulation across the prokaryotic cell membrane: K^+ uptake systems. In: *Handbook of Biological Physics Vol. 2* (Konings, W. N., Kaback, H. R., and Lolkema, J. S., eds.), pp. 473-499, Elsevier Science, Amsterdam.

5. Booth, I. R. (1985) Regulation of cytoplasmic pH in bacteria. *Microbiol. Rev. 49*, 359-378.

6. Schuldiner, S., and Padan, E. (1993) Na^+/H^+ antiporters in *Escherichia coli*. In: *Alkali cation transport systems in prokaryotes* (Bakker, E.P., ed.), pp. 25-51, CRC Press, Boca Raton, Florida.

7. Rhoads, D. B., and Epstein, W. (1978) Cation transport in *Escherichia coli*. IX. Regulation of K^+ transport. *J. Gen. Physiol. 72*, 283-295.

8. Measures, J. C. (1975) Role of amino acids in osmoregulation of nonhalophilic bacteria. *Nature 257*, 389.

9. Christian, J. H. B., and Waltho, J. A. (1962) Solute concentrations within cells of halophilic and non-halophilic bacteria. *Biochim. Biophys. Acta.. 65*, 506.

10. Kushner, D. J., and Kamekura, M. (1988) Physiology of halophilic bacteria. In: *Halophilic Bacteria, Vol. I*, Rodriguez-Valera, F. Ed. , CRC Press, Boca Raton, FL, 109.

11. Imhoff, J. F. (1988) Halophilic phototrophic bacteria. In: *Halophilic Bacteria, Vol. I*, Rodriguez-Valera, F. Ed. , CRC Press, Boca Raton, FL, 85.

12. Galinski E. A., Pfeiffer, H. P., and Truper, H. G. (1985) 1,4,5,6-Tetrahydro-2-methyl-4-pyrimidinecarboxylic acid. A novel cyclic amino acid from halophilic phototrophic bacteria of the genus *Ectothiorhodospira. Eur. J. Biochem. 149*, 135-139.

13. Larsen, P. I., Sydnes, L. K., Landfald, B., and Strom, A. R. (1987) Osmoregulation in *Escherichia coli* by accumulation of organic osmolytes: betaines, glutamic acid, and trehalose. *Arch. Microbiol. 147*, 1-7.

14. Dinnbier, U., Limpinsel, E., Schmid, R., and Bakker, E. P. (1988) Transient accumulation of potassium glutamate and its replacement by trehalose during adaptation of growing cells of *Escherichia coli* K-12 to elevated sodium chloride concentration. *Arch. Microbiol. 150*, 348-357.

15. Schleyer, M., Schmid, R., and Bakker, E. P. (1993) Transient, specific and extremly rapid release of osmolytes from growing cells of *Escherichia coli K-12* exposed to hypoosmotic shock. *Arch. Microbiol. 160*, 424-431.

16. Booth, I. R., Jones, M. A., McLaggan, D., Nikolaev, Y., Ness, L. S., Wood, C. M., Miller, S., Tötemeyer, S., and Ferguson, G. P. (1996) Bacterial ion channels. In: *Handbook of Biological Physics Vol. 2* (Konings, W.N., Kaback, H.R. and Lolkema, J.S., eds.), pp. 693-729, Elsevier Science, Amsterdam.

17. Ferguson, G. P., Nikolaev, Y., McLaggan, D., Maclean, M., and Booth, I. R. (1997) Survival during exposure to the electrophilic reagent N-ethylmaleimide in *Escherichia coli*: role of KefB and KefC potassium channels. *J. Bacteriol. 179*, 1007-1012.

18. Verkhovskaya, M. L., Verkhovsky, M. L., and Wikström, M. (1995) A novel antiporter activity catalyzing sodium and potassium transport from right-side-out vesicles of *E. coli. FEBS Lett. 363*, 46-48.

19. Berrier, C., Besnard, M., Ajouz, B., Coulombe, A., and Ghazi, A. (1996) Multiple mechanosensitive ion channels from *Escherichia coli*, activated at different threshold of applied pressure. *J. Membr. Biol. 151*, 175-187.

20. Bakker, E. P. (1993) Low-affinity K^+ uptake systems. In: *Alkali cation transport systems in prokaryotes* (Bakker, E.P., ed.), pp. 253-276, CRC Press, Boca Raton, Florida.

21. Stewart, L. M. D., Bakker, E. P., and Booth, I. R. (1985) Energy coupling to K^+ uptake via the Trk system in *Escherichia coli*: the role of ATP. *J. Gen. Microbiol. 131*, 77-85.

22. Bossemeyer, D., Schlösser, A., and Bakker, E. P. (1989) Specific caesium transport via the *Escherichia coli* Kup (TrkD) K^+ uptake system. *J. Bacteriol. 171*, 2219-2221.

23. Helmer, G. L., Laimins, L. A., and Epstein, W. (1982) Mechanism of potassium transport in bacteria. In: *Membranes and transport Vol. 2* (Martonosi, A.N., ed.), pp. 123-128, Plenum Publishing Corp., New York.

24. Ness, L. S. and Booth, I. R. (1999) Different loci for the regulation of the activity of the KefB and KefC glutathione-gated K^+ efflux systems. *J. Biol. Chem. 274*, 9524-9530.

25. Lucassen, M. (1998) Regulation des Kdp-Systems aus *Escherichia coli*: Biochemische Charakterisierung des Antwortregulators KdpE und Nachweis von Konformationsänderungen im Zuge der Aktivierung. Ph.D. Thesis, University of Osnabrueck, Osnabrueck, Germany.

26. Laimins, L. A., Rhoads, D. B., Altendorf, K., and Epstein, W. (1978) Identification of the structural proteins of an ATP-driven potassium transport system in *Escherichia coli*. *Proc. Natl. Acad. Sci. USA 75*, 3216-3219.

27. Epstein, W. (1985) The Kdp system: a bacterial K^+ transport ATPase. *Curr. Top. Membr. Transp. 23*, 153-175.

28. Rhoads, D. B., Waters, F. B., and Epstein, W. (1976) Cation transport in *Escherichia coli*. VIII. Potassium transport mutants. *J. Gen. Physiol. 67*, 325-341.

29. Hesse, J. E., Wieczorek, L., Altendorf, K., Reicin, A. S., Dorus, E., and Epstein, W. (1984) Sequence homology between two membrane ATPases, the Kdp-ATPase of *Escherichia coli* and the Ca^{2+}-ATPase of sarcoplasmic reticulum. *Proc. Natl. Acad. Sci. USA 81*, 4746-4750.

30. Siebers, A., and Altendorf, K. (1993) K^+-translocating Kdp-ATPases and other bacterial P-type ATPases. In: *Alkali cation transport systems in prokaryotes* (Bakker, E.P., ed.), pp. 225-252, CRC Press, Boca Raton, Florida.

31. Walderhaug, M. O., Polarek, J. W., Voelkner, P., Daniel, J. M., Hesse, J. E., Altendorf, K., and Epstein, W. (1992) Kdp D and KdpE, proteins that control expression of the *kdpABC* operon, are members of the two-component sensor-effector class of regulators. *J. Bacteriol. 174*, 2152-2159.

32. Polarek, J. W., Williams, G., and Epstein, W. (1992) The products of the *kdpDE* operon are required for expression of the Kdp ATPase of *Escherichia coli*. *J. Bacteriol. 174*, 2145-2151.

33. Altendorf, K., Voelkner, P., and Puppe, W. (1994) The sensor kinase KdpD and the response regulator KdpE control expression of the *kdpFABC* operon in *Escherichia coli*. *Res. Microbiol. 145*, 374-381.

34. Zimmann, P., Puppe, W., and Altendorf, K. (1995) Membrane topology of the sensor kinase KdpD of *Escherichia coli*. *J. Biol. Chem. 270*, 28282-28288.

35. Voelkner, P., Puppe, W., and Altendorf, K. (1993) Characterization of the KdpD protein, the sensor kinase of the K^+-translocating Kdp system of *Escherichia coli*. *Eur. J. Biochem. 217*, 1019-1026.

36. Heermann, R., Altendorf, K., and Jung, K. (1998) The turgor sensor KdpD of *Escherichia coli* is a homodimer. *Biochem. Biophys. Acta 1415*, 114-124.

37. Nakashima, K., Sugiura, A., Kanamaru, K., and Mizuno, T. (1993) Signal transduction between the two regulatory components involved in the regulation of the *kdpABC* operon in *Escherichia coli*: phosphorylation-dependent functioning of the positive regulator, KdpE. *Mol. Microbiol. 7*, 109-116.

38. Jung, K., Tjaden, B., and Altendorf, K. (1997) Purification, reconstitution, and characterization of KdpD, the turgor sensor of *Escherichia coli*. *J. Biol. Chem. 272*, 10847-10852.

39. Pedersen, P. L., and Carafoli, E. (1987) Ion motive ATPases. I. Ubiquity, properties, and significance to cell function. *Trends Biochem. Sci. 12*, 146-150.

40. Møller, J. V., Juul, B., and le Maire, M. (1996) Structural organization, ion transport, and energy transduction of P-type ATPases. *Biochim. Biophys. Acta 1286*, 1-51.

41. Greie, J.-C., and Altendorf, K. (2007) The K^+-translocating KdpFABC complex from *Escherichia coli*: a P-type ATPase with unique features. *J. Bioenerg. Biomembr. 39*, 397-402.

42. Laimins, L. A., Rhoads, D. B., and Epstein, W. (1981) Osmotic control of *kdp* expression in *Escherichia coli*. *Proc. Natl. Acad. Sci. USA 78*, 464-468.

43. Haupt, M., Bramkamp, M., Heller, M., Coles, M., Deckers-Hebestreit, G., Herkenhoff-Hesselmann, B., Altendorf, K., and Kessler, H. (2006) The holo-form of the nucleotide binding domain of the

KdpFABC complex from *Escherichia coli* reveals a new binding mode. *J. Biol. Chem. 281*, 9641-9649.

44. Taniguchi, K., Kaya, S., Abe, K., and Mardh, S. (2001) The oligomeric nature of Na/K-transport ATPase. *J. Biochem. (Tokyo) 129*, 335-342.

45. Chadwick, C. C., Goormaghtigh, E., and Scarborough, G. A. (1987) A hexameric form of the *Neurospora crassa* plasma membrane H$^+$-ATPase. *Arch. Biochem. Biophys. 252*, 348–356.

46. Rhee, K.-H., Scarborough, G. A., and Henderson, R. (2002) Domain movements of plasma membrane H$^+$-ATPase: 3D structures of two states by electron cryo-microscopy. *EMBO J. 21*, 3582–3589.

47. Bramkamp, M., and Altendorf, K. (2004) Functional modules of KdpB, the catalytic subunit of the Kdp-ATPase from *Escherichia coli. Biochemistry 43*, 12289-12296.

48. Axelsen, K. B., and Palmgreen, M. G. (1998) Evolution of substrate specificities in the P-type ATPase superfamily. *J. Mol. Evol. 46*, 84-101.

49. Bramkamp, M., and Altendorf, K. (2005) Single amino acid substitution in the putative transmembrane helix V in KdpB of the KdpFABC complex of *Escherichia coli* uncouples ATPase activity and ion transport. *Biochemistry 44*, 8260-8266.

50. Toyoshima, C., Nakasako, M., Nomura, H., and Ogawa, H. (2000) Crystal structure of the calcium pump of sarcoplasmic reticulum at 2.6 Å resolution. *Nature 405*, 647-655.

51. Anthonisen, A. N., Clausen, J. D., and Andersen. J. P. (2006) Mutational analysis of the conserved TGES loop of sarcoplasmic reticulum Ca^{2+}-ATPase. *J. Biol. Chem. 281*, 31572-31582.

52. Clarke, D. M., Loo, T. W., and MacLennan, D. H. (1990) Functional consequences of mutations of conserved amino acids in the beta-strand domain of the Ca^{2+}-ATPase of sarcoplasmic reticulum. *J. Biol. Chem. 265*, 14088-14092.

53. Aravind, L., Galperin, M. Y., and Koonin, E. V. (1998) The HD domain defines a new superfamily of metal-dependent phosphohydrolases. *Trends Biochem. Sci. 23*, 469-472.

54. Sazinsky, M. H., Mandal, A. K., Argüello, J. M., and Rosenzweig, A. C. (2006) Structure of the ATP Binding Domain from the *Archaeoglobus fulgidus* Cu$^+$-ATPase. *J. Biol. Chem. 281*, 11161–11166.

55. Toyoshima, C., and Mizutani, T. (2004) Crystal structure of the calcium pump with a bound ATP analogue. *Nature 430*, 529- 535.

56. Morth, J. P., Pedersen, B. P., Toustrup-Jensen, M. S., Sørensen, T. L., Petersen, J., Andersen, J. P., Vilsen, B., and Nissen, P. (2007) Crystal structure of the sodium-potassium pump. *Nature 450*, 1043-1049.

57. Olesen, C., Picard, M., Winther, A.-M., Gyrup C., Morth, J. P., Oxvig, C., Møller, J. V., and Nissen, P. (2007) The structural basis of calcium transport by the calcium pump. *Nature 450*, 1036-1042.

58. Rice, W. J., Young, H. S., Martin, D. W., Sachs, J. R., and Stokes, D. L. (2001) Structure of the Na$^+$,K$^+$-ATPase at 11 Å resolution: comparison with Ca^{2+}-ATPase in E1 and E2 states. *Biophys. J. 80*, 2187–2197.

59. Toyoshima, C., and Nomura, H. (2002) Structural changes in the calcium pump accompanying the dissociation of calcium. *Nature 418*, 605-611.

60. Toyoshima, C., Nomura, H., and Sugita, Y. (2003) Crystal structures of Ca^{2+}-ATPase in various physiological states. *Ann. N.Y. Acad. Sci. 986*, 1-8.

61. Hilge, M., Siegal, G., Vuister, G. W., Güntert, P., Gloor, S. M., and Abrahams, J. P. (2003) ATP-induced conformational changes of the nucleotide-binding domain of Na,K-ATPase. *Nat. Struct. Biol. 10*, 468-474.

62. Håkansson, K. O. (2003) The crystallographic structure of Na,K-ATPase N-domain at 2.6A resolution. *J. Mol. Biol. 33*, 21175-21182.

63. Dmitriev, O. Y., Tsivkovskii, R., Abildgaard, F., and Lutsenko, S. (2006) NMR assignment of the Wilson disease associated protein N-domain. *J. Biomol. NMR. 36*, Suppl 1:61.

64. Haupt, M., Bramkamp, M., Coles, M., Altendorf, K., and Kessler, H. (2004) Inter-domain motions of the N-domain of the KdpFABC complex, a P-type ATPase, are not driven by ATP-induced conformational changes. *J. Mol. Biol. 342*, 1547–1558.

65. Bramkamp, M., Altendorf, K., and Greie, J.-C. (2007) Common patterns and unique features of P-type ATPases: a comparative view on the KdpFABC complex from *Escherichia coli. Mol. Membr. Biol. 24*, 375-386.

66. Kimura, Y., and Inui, M. (2002) Reconstitution of the cytoplasmic interaction between phospholamban and Ca^{2+}-ATPase of cardiac sarcoplasmic reticulum. *Mol. Pharmacol. 61*, 667-673.

67. Kühlbrandt, W., Zeelen, J., and Dietrich, J. (2002) Structure, mechanism and regulation of the *Neurospora* plasma membrane H$^+$-ATPase. *Science. 297*, 1692-1696.

68. Therien, A. G., Karlish, S. J. D., and Blostein, R. (1999) Expression and functional role of the γ subunit of the Na, K-ATPase in mammalian cells. *J. Biol. Chem. 274*, 12252-12256.

69. Kühlbrandt, W. (2004) Biology, structure and mechanism of P-type ATPases. *Nat. Rev. Mol. Cell. Biol. 5*, 282-295.

70. Bramkamp, M., Gaßel, M., and Altendorf, K. (2004) FITC Binding site and p-nitrophenyl phosphatase activity of the Kdp-ATPase of *Escherichia coli*. *Biochemistry 43*, 4559-4567.

71. Haupt, M., Bramkamp, M., Coles, M., Kessler, H., and Altendorf, K. (2005) Prokaryotic Kdp-ATPase: recent insights into the structure and function of KdpB. *J. Mol. Microbiol. Biotechnol. 10*, 120-131.

72. Kubala, M. (2006) ATP-binding to P-type ATPases as revealed by biochemical, spectroscopic, and crystallographic experiments. *Proteins 64*, 1-12.

73. Abu-Abed, M., Mal, T. K., Kainosho, M., MacLennan, D. H., and Ikura, M. (2002) Characterization of the ATP-binding domain of the sarco(endo)plasmic reticulum Ca^{2+}-ATPase: probing nucleotide binding by multidimensional NMR. *Biochemistry. 41*, 1156-1164.

74. Bertrand, J., Altendorf, K., and Bramkamp, M. (2004) Amino acid substitutions in putative selectivity filter regions III and IV in KdpA alter ion selectivity of the KdpFABC complex from *Escherichia coli*. *J. Bacteriol. 186*, 5519-5522.

75. Buurman, E. T., Kim, K. T., and Epstein, W. (1995) Genetic evidence for two sequentially occupied K$^+$ binding sites in the Kdp transport ATPase. *J. Biol. Chem. 270*, 6678-6685.

76. Schrader, M., Fendler, K., Bamberg, E., Gaßel, M., Epstein, W., Altendorf, K., and Dröse, S. (2000) Replacement of glycine 232 by aspartic acid in the KdpA subunit broadens the ion specificity of the K$^+$-translocating KdpFABC complex. *Biophys. J. 79*, 802-813.

77. van der Laan, M., Gaßel, M., and Altendorf, K. (2002) Characterization of amino acid substitutions in KdpA, the K$^+$-binding and -translocating subunit of the KdpFABC complex of *Escherichia coli*. *J. Bacteriol. 184*, 5491-5494.

78. Durell, S. R., Bakker, E. P., and Guy, H. R. (2000) Does the KdpA subunit from the high affinity K$^+$-translocating P-type Kdp-ATPase have a structure similar to that of K$^+$ channels? *Biophys. J. 77*, 775-788.

79. Doyle, D. A., Morais Cabral, J., Pfuetzner, R. A., Kuo, A., Gulbis, J. M., Cohen, S. L., Chait, B. T., and MacKinnon, R. (1998) The structure of the potassium channel: molecular basis of K$^+$ conduction and selectivity. *Science 280*, 69-77.

80. Becker, D., Fendler, K., Altendorf, K., and Greie J.-C. (2007) The conserved dipole in transmembrane helix 5 of KdpB in the *Escherichia coli* KdpFABC P-type ATPase is crucial for coupling and the electrogenic K$^+$-translocation step. *Biochemistry 46*, 13920-13928.

81. Gaßel, M., and Altendorf, K. (2001) Analysis of KdpC of the K+-transporting KdpFABC complex of Escherichia coli. Eur. J. Biochem. 268, 1772-1781.

82. Ahnert, F., Schmid, R., Altendorf, K., and Greie, J.-C. (2006) ATP binding properties of the soluble part of the KdpC subunit from the *Escherichia coli* K$^+$-transporting KdpFABC P-type ATPase. *Biochemistry 45*, 11038-11046.

83. Gaßel, M., Möllenkamp, T., Puppe, W., and Altendorf, K. (1999) The KdpF subunit is part of the K$^+$-translocating Kdp complex of *Escherichia coli* and is responsible for stabilization of the complex in vitro. *J. Biol. Chem. 274*, 37901-37907.

84. Iwane, A. H., Ikeda, I., Kimura, Y., Fujiyoshi, Y., Altendorf, K., and Epstein, W. (1996) Two-dimensional crystals of the Kdp-ATPase of *Escherichia coli*. *FEBS-Lett. 396*, 172-176.

85. Hu, G. B., Rice, W. J., Dröse, S., Altendorf, K., and Stokes, D. L. (2008) Three-dimensional structure of the KdpFABC complex of *Escherichia coli* by electron tomography of two-dimensional crystals. *J. Struct. Biol. 161*, 411-418.

86. Post, R. L., Hegyvary, C., and Kume, S. (1972) Activation by adenosine triphosphate in the phosphorylation kinetics of sodium and potassium ion transport adenosine triphosphatase. *J. Biol. Chem. 247*, 6530-6540.

87. Albers, R. W. (1967) Biochemical aspects of active transport. *Annu. Rev. Biochem. 36*, 727-756.

88. Horisberger, J. D. (2004) Recent insights into the structure and mechanism of the sodium pump. *Physiology 19*, 377-387.

89. Kanazawa, T., Suzuki, H., Daiho, T., and Yamasaki, K. (1995) Fluorometric study on conformational changes in the catalytic cycle of sarcoplasmic reticulum Ca^{2+}-ATPase. *Biosci. Rep. 15*, 317-326.

90. Karlish, S. J., Goldshleger, R., Tal, D. M., Capasso, J. M., Hoving, S., and Stein, W. D. (1992) Identification of the cation binding domain of Na/K-ATPase. *Acta. Physiol. Scand. Suppl. 607*, 69-76.

91. Shin, J. M., Besancon, M., Bamberg, K., and Sachs, G. (1997) Structural aspects of the gastric H,K-ATPase. *Ann. N. Y. Acad. Sci. 834*, 65-76.

CHAPTER I

K$^+$-Translocating KdpFABC P-Type ATPase from

Escherichia coli Acts as a Functional and Structural Dimer

Thomas Heitkamp *, René Kalinowski §, Bettina Böttcher $^#$, Michael Börsch ‡,

Karlheinz Altendorf *, and Jörg-Christian Greie *
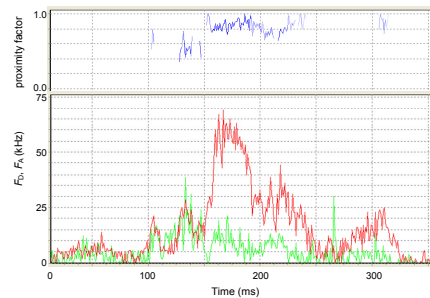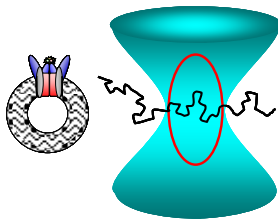
*   Universität Osnabrück, Fachbereich Biologie/Chemie, Arbeitsgruppe Mikrobiologie, 49069
     Osnabrück, Germany

§   Scriptor Dokumantations Service GmbH, Krackser Str. 12C, 33659 Bielefeld, Germany

EMBL Heidelberg, Meyerhofstraße 1, 69117 Heidelberg, Germany

‡   3. Physikalisches Institut, Pfaffenwaldring 57, 70550 Stuttgart, Germany

REFERENCE

This chapter is already published as:

NOTE

This chapter is based in part on the results obtained by former results, which were described in the diploma thesis of René Kalinowski (2003, Universität Osnabrück) and are listed in the following. The products resulting from oxidative cross-linking of intrinsic cysteines of KdpB were characterized with respect to the formation of intermolecular and intramolecular cross-links. Furthermore, a gel filtration experiment using cross-linked and non-cross-linked KdpFABC complexes demonstrated the co-elution of both populations. These experiments were reproduced and extended by the quantification of cross-link products and the determination of the molecular weight of the co-elution peak.

Furthermore, plasmids encoding cysteine-free *kdpA* and *kdpB* mutants were kindly provided by Doris Becker. In this study, these plasmids were used to generate the pGS4ΔCys plasmid for the production of a KdpFABC complex lacking all cysteines.

Finally, homology modeling of KdpB was carried out by Henrik Strahl. In the present chapter, the corresponding pdb-file was used to generate Figure 1.

CHAPTER II

Solution Structure of the KdpFABC P-type ATPase

from *Escherichia coli*

by Electron Microscopic Single Particle Analysis

Thomas Heitkamp *, Bettina Böttcher [§], and Jörg-Christian Greie *

*   Universität Osnabrück, Fachbereich Biologie/Chemie, Arbeitsgruppe Mikrobiologie,
     49069 Osnabrück, Germany

[§]   University of Edinburgh, School of Biological Sciences, Mayfield Road,
     Edinburgh EH9 3JR, UK

REFERENCE

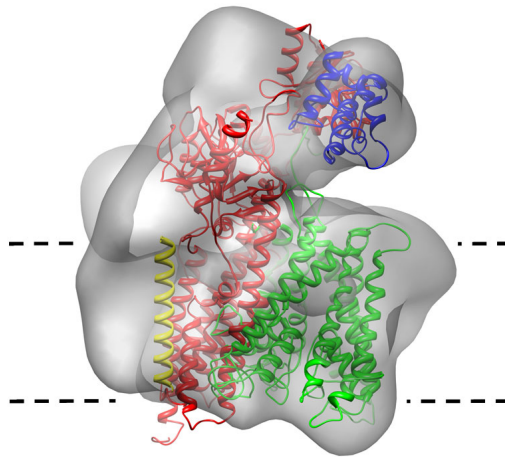This chapter is already published in electronic form as:

Heitkamp, T., Böttcher, B., and Greie, J-C. (2009) Solution structure of the KdpFABC P-type ATPase from Escherichia coli by electron microscopic single particle analysis. *J. Sruct. Biol.* **DOI**:10.1016/j.jsb.2009.02.016.

NOTE

This chapter includes three structural models made by Henrik Strahl. These are the homology models of KdpB and KdpA as well as the *ab initio* model of KdpC$_{90-188}$. In the case of KdpB, the corresponding pdb-files were slightly modified in this study in order to fill some structural gaps. Subsequently, the pdb-files were used in the present thesis for fitting of the models into the 3D map obtained from electron microscopic single particle analysis as well as for generating Figure 1.

C H A P T E R   I I I

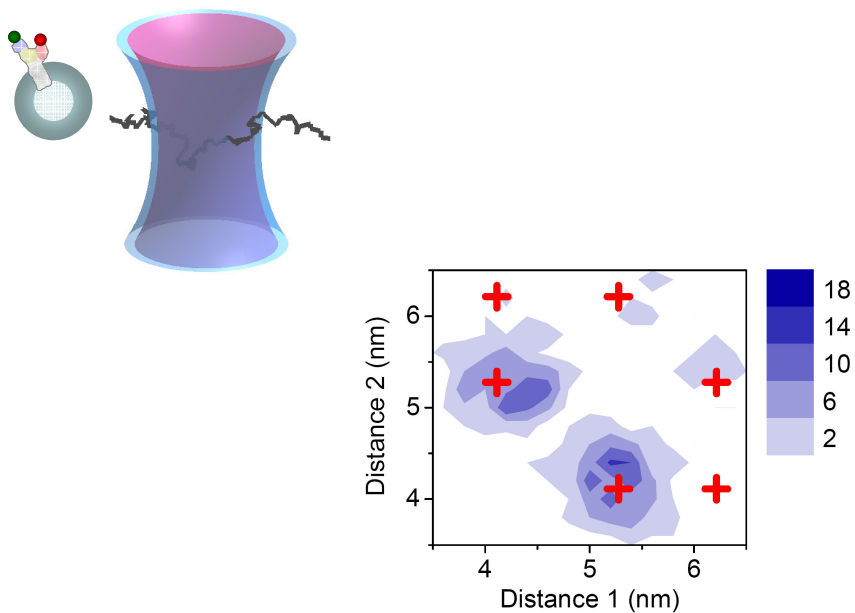# Conformational Dynamics of the KdpFABC P-type ATPase

from *Escherichia coli*

Revealed by Single Molecule ALEX-FRET

Thomas Heitkamp *, Nawid Zarrabi [§], Michael Börsch [§], and Jörg-Christian Greie *

*   Universität Osnabrück, Fachbereich Biologie/Chemie, Arbeitsgruppe Mikrobiologie, 49069
     Osnabrück, Germany

[§]   3. Physikalisches Institut, Pfaffenwaldring 57, 70550 Stuttgart, Germany

ABSTRACT

P-type ATPases share a structurally and biochemically well-studied reaction cycle, which includes dynamic movements of cytoplasmic domains. Although a lot of structural data on P-type ATPases in different substeps of the reaction cycle is yet available, domain movements have so far never been shown directly within the catalytically active enzyme. In the present study, the KdpFABC complex from *Escherichia coli*, which is a rather unique multi-subunit, K^+-translocating P-type ATPase, was used to directly observe these domain movements within the working enzyme. The two large cytoplasmic domains of KdpB, which shares the structural features of P-type ATPases, were site-directedly labeled with different fluorophores. By use of single molecule FRET on freely diffusing proteoliposomes combined with an alternating laser excitation scheme (ALEX), we were able to measure the distances and, thus, dynamic fluctuations between these domains. Three different distances, namely S1 (~5 nm), S2 (~4 nm) and S3 (~6 nm), could be measured in either the catalytically active or in the vanadate- as well as in the OCS-inhibited states. Thereby, the S1 and the S2 distances are in well accord with the expected distances of an open and closed conformation of KdpB. The S3 distance occurred rather seldom and traversed only to the S1 conformation, thereby indicating a conformation, which merely resides from the high flexibility of one domain and which is not part of the reaction cycle itself. Furthermore, dwell times of both the S1 and S2 state could be determined for both the non-inhibited and the inhibited complex. These dwell times indicate that despite the protein is biochemically blocked, it retains a high grade of flexibility.

INTRODUCTION

One of the most fundamental prerequisites of life is the generation and maintenance of ion gradients across biological membranes. These gradients are used for processes like energy conversion, transport and maintenance of a cell turgor and pH. For both the generation and maintenance of these ion gradients, active ion transport processes are necessary. In the case of high cation gradients, the corresponding transport is mainly catalyzed by P-type ATPases, which are characterized by a primary ion transport across membranes at the expense of ATP (*1*) and which are broadly distributed among prokaryotes and eukaryotes (*2*). Because of their great importance, especially eukaryotic representatives such as the sarco(endo)plasmatic Ca^{2+}-ATPase (SERCA), the Na^+,K^+-ATPase of animal cells and the H^+,K^+-ATPase of the gastric mucosa have been investigated in great detail with respect to both structure and function (*3-10*).

   The multisubunit potassium-transporting KdpFABC complex of *Escherichia coli* also belongs to the family of P-type ATPases. However, it exhibits some unique features, which are reflected by the subunit composition of the complex. Only the KdpB subunit (72 kDa) shares the structural and functional features of P-type ATPases according to their mode of ATP hydrolysis (Figure 1A). Like all members of this family, KdpB is composed of one transmembrane domain (TM-domain) and three soluble domains, referred to as the nucleotide binding domain (N-domain), phosphorylation domain (P-domain) and actuator domain (A-domain) (Figure 1A). Furthermore, KdpB features the formation of a transient phosphointermediate by autophosphorylation of a conserved aspartic acid residue, which separates this class of enzymes from other ATPases (*11*). However, the lack of ion binding sites in the TM-domain and the presence of a separate subunit, which is responsible for the translocation of the substrate, the KdpA polypeptide (59 kDa), is a unique feature among P-type ATPases (*12-15*). Based on the analyses of sequence alignments it has been concluded that KdpA is evolutionary derived from a homotetrameric MPM-type (membrane/P-loop/membrane) K^+ channel by gene duplication and fusion events, thus assigning KdpA to the superfamily of prokaryotic MPM-type K^+ channel proteins (*15, 16*). Homology modelling of KdpA led to the notion that KdpA consists of eight central transmembrane helices forming four consecutive MPM-motifs, which are flanked by an N-terminal and a C-terminal transmembrane helix, thus summing up to 10 transmembrane helices in KdpA (*13, 16*). Due to its unique division of labor, the KdpFABC complex shows a special energy coupling mechanism, which is still under investigation. KdpB exhibits a highly conserved dipole within transmembrane helix five of the TM-domain, which is crucial for the coupling of ATP-hydrolysis in KdpB to ion transport in KdpA (*17*). The KdpC subunit (21 kDa) is reported to be essential for the activity of the complex (*18*), and comprises one N-terminal transmembrane helix followed by a large

cytoplasmatic extension. It has recently been shown that the soluble part is capable of ATP binding via the ribose moiety of the nucleotide, which led to the suggestion that KdpC acts as a catalytical chaperone in a cooperative ATP-binding together with KdpB (*19*). The KdpF subunit (3 kDa) consists of only one transmembrane helix with no further cytoplasmic or periplasmic extensions. However it is an integral part of the KdpFABC complex and is thought to play a role in stabilization of the complex, especially *in vitro* (*20*).

Despite the differences to other P-type ATPases regarding the subunit organization of KdpFABC, the reaction cycles are essentially equal. The characteristic feature of the reaction cycle of all P-type ATPases is the presence of two major structural and biochemical different states, the open E1 state and the closed E2 state (*1*) (Figure 1A). Binding of ATP to the E1 state and subsequent phosphorylation of the conserved aspartate residue in the P-domain triggers the formation of the E1~P state. The conversion into the E2-P state is coupled to the transport of the ions across the membrane. Subsequent dephosphorylation of the aspartate residue results in the formation of the E2 state. During this reaction cycle, the N- and A-domains are supposed to undergo rather large swivel and tilt movements (*3, 6*). The reaction cycle with two main conformational states involving phosphorylation, substrate binding and release, is put together in a reaction scheme, which became prominent under the name Albers-Post mechanism (*21, 22*).

However, conformational changes between E1 and E2 have so far only been derived rather indirectly by the crystallization of locked-in protein conformations representing substeps within the reaction cycle, by the modulation of intrinsic tryptophan fluorescence or by proteolytic digestion experiments (For overview: *23-27*). Additionally, only rudimentary information is yet available about the dwell times of the E1 and E2 state and the flexibility of the N- and A-domain in these states of both the catalytically active and the inhibited enzyme.

In this work, we used single molecule FRET with alternating laser excitation (ALEX) to directly measure the conformational changes within KdpB during ATP hydrolysis. Purified KdpFABC complexes were reconstituted into liposomes and subsequently labeled with fluorescent maleimides at both the N- and the A-domain. The ALEX-approach allowed for the simultaneous recording of fluorescence intensity and fluorescence lifetime in a time-dependent manner. Furthermore, the alternating excitation of both the donor and the acceptor rendered the discrimination of FRET events from photophysical effects possible. Hidden-Markov-Models have been evaluated for the detection of fast fluctuations in a millisecond time scale. Additionally, the results of the Hidden-Markov-Model were scrutinized by manual analysis. With this approach, the distances and dwell times for three conformational states in the working cycle as well as in the *ortho*-vanadate and the OCS-inhibited (oligocyclic suboxides) complex were determined.

EXPERIMENTAL PROCEDURES

Bacterial Strains and Growth Conditions.

For the expression of *kdpFABC*-wild type and mutants, strain TKW3205 (*ΔkdpABC'05 nagA-trkA405 trkD1 Datp706*) was used, which contains no functional K$^+$ uptake system but still carries the chromosomal *kdpDE* operon for K$^+$-induced *kdpFABC* expression. This strain was transformed with one of the plasmids listed in the following section. All plasmids are derivatives of plasmid pGS4 carrying the *kdpFABC* genes under control of the *kdp* promotor. In addition, the *kdpA* gene comprises a 3' (CATCAC)$_7$ extension coding for a C-terminal His$_{14}$ tag. TKW3205 cells transformed with pGS4 derivatives were grown as described in ref *28*.

Generation of *kdpB* Mutants.

For the site-specific incorporation of fluorescent FRET labels, all native cysteines in the KdpFABC complex except residues C261 and C609 of KdpB were replaced by alanine or serine according to ref *28* (For primer list: Appendix, Table 1). The resulting plasmid pGS4ΔCys-KdpB(C261/C609) was used as template for the site-directed introduction of cysteine residues at the position of the exposed glycine-150 within the A-domain and/or at the position of the exposed alanine-407 in the N-domain of KdpB (Figure 1). The corresponding PCR products were cloned into pGS4ΔCys-KdpB(261C/609C) via the restriction sites *Mfe* I and *Hpa* I in case of G150C or via the *Cla* I and *Bam*H I restriction sites in case of A407C, resulting in the three plasmids pGS4ΔCys-KdpB(C261/C609/G150C), pGS4ΔCys-KdpB(C261/C609/A407C) and pGS4ΔCys-KdpB(C261/C609/G150C/A407C). For further information about the used plasmids, see also Appendix, Table 2.

Purification of the KdpFABC Complex.

His$_{14}$-tagged KdpFABC complexes were purified from TKW3205 cells via metal chelate affinity chromatography followed by size exclusion chromatography as described in ref *28* using the following modifications. Immediately after cell lysis, the protease inhibitor cocktail complete EDTA-free (Roche) was added following the manufacturer's instructions. In order to avoid protein interactions due to cystine formation, all subsequent buffers contained 1 mM β-mercaptoethanol. Furthermore, solubilized proteins were applied to Ni-NTA agarose (Quiagen) pre-equilibrated with buffer containing 20 mM instead of 10 mM imidazole followed by washing steps with the same buffer containing 30 mM imidazole and 43 mM imidazole prior to the elution of KdpFABC with 135 mM imidazole. Concentrated Ni-NTA fractions were loaded on a 10/30 Superdex-S200 column (Amersham Biosciences) equilibrated with 50 mM Tris-HCl pH 7.0, 10 % glycerol,

150 mM NaCl, 0.5 mM PMSF, 0.2 % (v/v) aminoxide WS-35 and developed at a flow rate of 0.5 mL/min. Protein-containing peak fractions were again pooled and concentrated according to ref *28*.

Reconstitution of the KdpFABC Complex.

Reconstitution of KdpFABC into proteoliposomes was carried out as described in (*28*).

ATPase Activity Assay.

ATPase activities of purified KdpFABC complexes were determined using the microtiter plate assay of Henkel *et al.* (*29*) following the modifications described in (*30*). For the analyses of ATPase activities in proteoliposomes, measurements were carried out in the absence of detergent. A total of 0.5 μg of purified protein was routinely used for a single measurement.

Fluorometric Transport Measurements:

The fluorometric transport measurements with reconstituted KdpFABC complexes were carried out in 1 mL of 50 mM Tris-HCl, pH 7.5, 50 mM KCl, 2 mM $MgCl_2$ as described (*30, 31*) by use of an SLM-Aminco 8100 spectrofluorometer (SLM-Aminco) at an excitation wavelength of 650 nm, an emission wavelength of 675 nm, a monochromator bandwidth of 4 nm and an integration time of 1 s. The reaction mixture containing 10 μL of proteoliposomes was supplied with 1 μM $DiSC_3(5)$. The addition of 1 mM ATP initiated the transport reaction. *Ortho*-vanadate (100 μM) served as a specific P-type ATPase inhibitor, whereas 1 μM valinomycin was used as a K^+-specific uncoupling ionophore.

Fluorescence Labeling of Cysteines.

Labeling of cysteines with fluorescent maleimides was done essentially according to ref *28*. In this study, the fluorescent dyes ATTO 655-maleimide (ATTO-TEC) and Alexa 488-maleimide (Molecular Probes) were used. Labeling specificity was determined by SDS-PAGE with subsequent visualization under UV-light. Labeling efficiency was calculated using the KdpFABC concentration determined via SDS-PAGE as described above together with the fluorophor absorption at 493 nm for Alexa 488 ($\varepsilon = 72,000 \ M^{-1} \ cm^{-1}$) and at 663 nm for ATTO 655 ($\varepsilon = 125,000 \ M^{-1} \ cm^{-1}$). To exclude eventual shifts in the spectra of the fluorophores upon binding to the protein moiety, the absorbance spectra of the labeled KdpFABC complexes were measured photometrically. In order to minimize light scattering effects during the absorbance measurements, a corresponding aliquot of the labeled proteoliposome sample was solubilized with 2 % (v/v) Triton-X-100 as a control. Finally, labeled proteoliposomes were diluted with preformed plain control liposomes containing no protein to adjust a KdpFABC/liposome ratio of 0.4. Subsequently, solubilisation with 1 % (w/v) Triton-X-100 and consecutive detergent removal as described in (*28*)

allowed for an equal distribution of the reconstituted and labeled KdpFABC complexes. Proteoliposomes were stored at 4 °C and were used for FRET measurements within one week.

ALEX-FRET Analysis.

Single molecule FRET measurements were performed on a custom-designed confocal microscope based on an inverted Olympus IX 71 (For overview: Supplemental Figure I). Droplets (50 μL) of the labeled proteoliposomes were placed on a glass coverslip. For excitation, fiber-coupled ps-pulsed laser sources were used at 488 nm (PicoTa 490, operated at 40 MHz repetition rate; Picoquant, Berlin, Germany) and 635 nm (LDH-P-C-635B, 40 MHz repetition rate; Picoquant), which were triggered by the laser driver unit PDL-808 SEPIA (2-channel version, Picoquant). Excitation power of the PicoTA 490 was adjusted to 150 μW, and the excitation power of the red laser was reduced to 25 μW. For alternating laser excitation, the red laser pulse was delayed by 15 ns with respect to the 488 nm pulse using a prolonged trigger cable. The laser beams were compressed to beam diameters of about 3 mm for the solution measurements and overlaid by reflection from (488 nm beam) or transmission through (635 nm beam) a dichroic beam splitter (DXCR 540, AHF, Tübingen, Germany). In epi-fluorescence configuration, both beams were re-directed by a dual band dichroic filter (HC dual line beam splitter 488/633-638, AHF) and focused in the buffer droplet by use of a water immersion objective (UPlanSApo 60xW, 1.2 N.A., Olympus, Hamburg, Germany). To prove the co-localization of the overlaid excitation foci, a sample with immobilized fluorescent microbeads on a glass cover slide was scanned in three dimensions, and resulting image stacks from the two lasers were compared. Fluorescence of FRET donor and acceptor dyes were simultaneously detected by two avalanche photodiodes (AQR-14, Perkin Elmer, Germany). After passing the 150 μm pinhole, fluorescence was separated by a dichroic HQ640LP mirror (AHF) and detected in the FRET donor channel at a bandwidth of 497 nm to 567 nm (interference filter HQ532/70, AHF) and in the acceptor channel above 665 nm (long pass filter HQ665LP, AHF). Single photons were recorded by a time-correlated single photon-counting PC card (SPC-630, Becker&Hickl, Berlin, Germany) combined with an 8-channel router (HRT-82, Becker&Hickl). For triggering the SPC-630 card, the trigger output of the PDL-808 SEPIA was used in combination with an LTT100 sync adaptor (Picoquant). Photons were stored in the FIFO mode of the TCSPC card. Therefore, the so-called "macro time" of each photon had a time resolution of 50 ns, which was used for 1 ms binning of the fluorescence intensity data and for fluorescence correlation spectroscopy. The "micro time" of each photon (arrival time with respect to the laser pulses) was used to calculate the fluorescence lifetime histograms within each selected photon burst or time bin. Furthermore, the "micro time" information of the photons in the FRET acceptor channel was applied to discriminate between photons detected as a result of FRET following excitation at 488 nm and photons originating from the direct excitation of the FRET

acceptor with the red laser pulse. Time trajectories of the FRET signals as well as the FRET acceptor control were analyzed by the custom-designed software Burst_Analyzer (*32*). At first, photon bursts of KdpFABC-containing labeled proteoliposomes were selected by fluorescence intensity thresholds using the acceptor control time trajectory. That is, each burst had to exceed 20 counts per ms for direct excitation of the acceptor at an average frequency of 5 kHz (i.e., 5000 counts per second or 5 counts per millisecond, respectively) throughout the burst. Thereby, photon bursts showing apparent FRET merely caused by spectral fluctuations of the FRET donor in the absence of an acceptor could effectively be excluded from further analysis. *Vice versa*, photon burst originating from the direct excitation of the FRET acceptor at 635 nm could also be removed by a minimum threshold of 5 kHz on average due to the lack of signal in the corresponding donor channel at 488 nm.

RESULTS

Single molecule FRET techniques represent a useful tool for the determination of intra- and intermolecular movements in the range of a few nanometers. For example, the rotation of the γ and the ε subunit of the F_1F_O-ATP-Synthase from *Escherichia coli* were analyzed in detail by single molecule FRET measurements (*32-35*). In the case of P-type ATPases, rather large movements of the N- and A-domain are generally assumed. Crystal structures of P-type ATPases like SERCA or the Na^+,K^+-ATPase caught in different substeps of the reaction cycle fortify this model (*3-6, 10*). Nevertheless, these movements have never been shown directly in the catalytically active enzyme. Hence, although these conformational changes are supposed to be highly dynamic, no detailed information is yet available on the actual distance changes between the cytosolic domains of a P-type ATPase during its catalytic cycle as well as on their dwell times and on their overall flexibility.

At this point, single molecule FRET measurements allow for a direct analysis of distance changes between two specific fluorescently labeled positions in a native environment and, in particular, in the active enzyme. The FRET efficiency highly depends on the distance between the donor and acceptor fluorophores as described by the Förster equation (*36*)

$$E_{\text{FRET}} = \frac{R_0^6}{R_0^6 + r_{\text{DA}}^6} \tag{1}$$

with R_0 representing the Förster radius (i.e., the fluorophore distance at which 50 % energy transfer occurs) and r_{DA} representing the actual distance between the donor and acceptor. Therefore, if the

donor and acceptor fluorophores are positioned around the Förster radius, even small changes in the distance result in strong modulations of the FRET efficiency. To achieve measurements on the single molecule level, the detection volume is set to a size of only a few femtoliters by diffraction-limited focusing of a laser beam with a microscope objective into the sample buffer (Figure 1B and Supplemental, Figure I). In principle, this enables the counting and characterization of each fluorescently labeled enzyme complex traversing the laser spot. The emitted fluorescence is stored as individual, time-separated photon bursts.
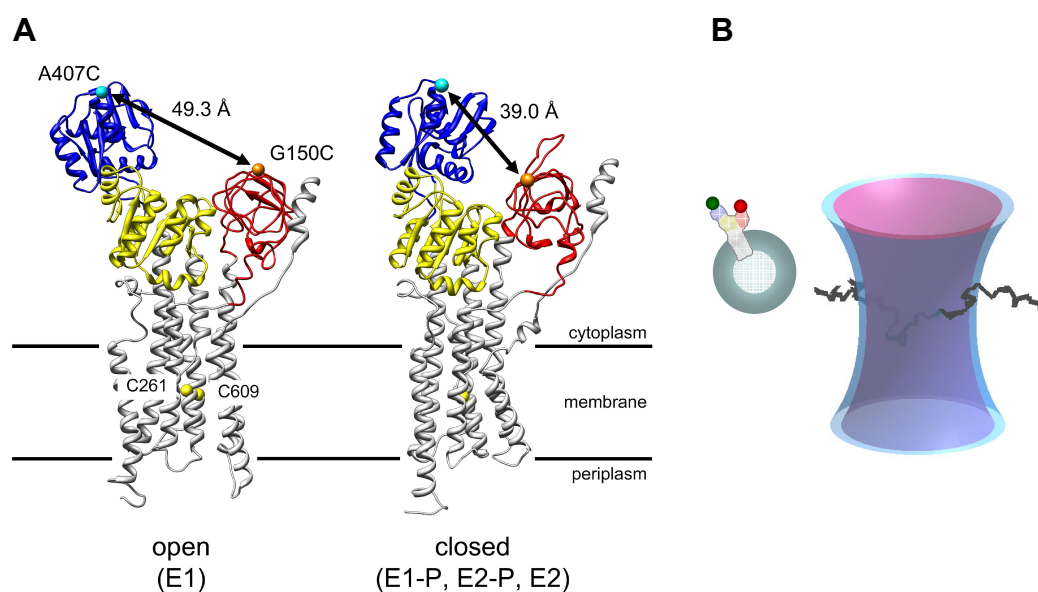
Figure 1: Supposed structures and single-molecule FRET of reconstituted KdpFABC. (A) Two possible conformations of KdpB with two cysteine residues introduced in the nucleotide binding domain (N-domain, blue; position 407) and in the actuator domain (A-domain, red, position 150) for labelling and single-molecule FRET analyses. The distances between these two positions are highlighted. The biochemical states belonging to the open and closed structural states are given in parentheses. Structures were modeled against published PDB files (1SU4, 1T5T) of SERCA (*3, 36*). (B) Confocal single-molecule FRET detection of freely diffusing proteoliposomes in solution with alternating two-colour laser excitation.

In case of KdpFABC, enzyme complexes were labeled with both donor (Alexa 488) and acceptor (ATTO 655) in order to determine FRET efficiencies modulated by distance changes between the A- and N-domain of KdpB. The R_0 of the Alexa 488/Atto 655 pair of dyes chosen as maleimide derivatives is 5.0 nm. This perfectly matches the proposed distance between the two residue positions taken for labeling, which is supposed to shift from 3.9 to 4.9 nm during the reaction cycle (Figure 1A). For the site-specific incorporation of the fluorescent labels at the N- and A-domain of KdpB, all native cysteines beside KdpB-C261 and KdpB-C609, which turned out to be essential for enzyme activity but could not be labeled due to their membrane-embedded location (Supplemental, Figure II), were substituted by alanine or serine depending upon the proposed hydrophobicity of the environment. Subsequently, cysteines were introduced at positions 150 and 407 (Figure 1A), which could selectively be labeled with fluorescent maleimides (Supplemental,

Figure II). Both the exchange of the wildtype cysteines as well as the introduction of new cysteine residues had no influence on enzyme activity as demonstrated by analyses of ATP-driven, *ortho*-vanadate-sensitive K^+ transport in proteoliposomes (Supplemental, Figure III).The reconstituted complexes were simultaneously labeled with both the donor and acceptor dye, which resulted in a stochastic labeling of individual KdpB with either only one dye or two dyes attached. Binding of the fluorescent dyes to the protein had only negligible effects on the absorbance spectra of the dyes and, as a consequence, should also not affect the fluorescence properties of the dyes (Supplemental, Figure IV). The labeling ratios for each fluorophore range from 20 to 30 %, which are rather high for reconstituted, highly diluted protein. However, only in case of a mixed labeling with both donor and acceptor at the same KdpB, FRET is supposed to occur. In order to separate these FRET events from false signals residing from KdpB only labeled with either Alexa 488 or Atto 655, the alternating laser excitation approach was used (ALEX).

As the protein traversed the confocal excitation volume, a burst of fluorescence photons was created (Figure 1B, Figure 2B-D). The diffusion time of the KdpFABC proteoliposomes was about 30 ms as calculated from the autocorrelation function of the FRET acceptor (directly excited at 635 nm), which corresponded to liposome diameters between 100 and 200 nm as expected from the sizing procedure. In order to prevent FRET artifacts caused by rotational immobility of the fluorescence labels, the anisotropy of Alexa 488 bound at either the A- or N-domain was determined (Supplemental, Figure V). Only the dye bound at the A-domain showed a slight anisotropy, which could, however, be neglected because of the free mobility of the dye bound at the N-domain. Because the mobility of fluorescent maleimides mainly depends on the protein environment, the ATTO 655 dye was not tested extra.

Resulting typical time traces as a result of donor excitation at 488 nm are shown in Figures 2B-D. The concomitant presence of donor, FRET and acceptor signal accounted for real FRET events instead of photophysical effects caused by the donor label. This is especially important in the case of low labeling efficiencies, which enhance the possibility of donor-only labeled complexes. The intensities of donor, FRET and acceptor signal transiently increased when a proteoliposome traversed the detection volume. The observed fluctuations in intensity of the measured time traces result from two major effects. First, fluctuating fluorescence intensities for the FRET donor (green trace) and the FRET acceptor (red trace) can be caused by Brownian motion of the KdpFABC complex, which affects the position-dependent detection efficiency within the confocal volume. Simultaneously, the FRET acceptor intensities (orange trace) are fluctuating when excited with 635 nm. Second, conformational fluctuations change the intramolecular donor/acceptor distance and, accordingly, the FRET transfer efficiency (equation 1), which leads to anti-correlated fluctuations in the fluorescence intensities of FRET donor and acceptor. From the

corrected intensity ratios at every timestep and the given Förster radius, the distance trajectory (Figure 2B-D, blue traces with standard deviation in light blue) between the FRET donor and acceptor at the N- and A-domain was calculated. In the presence of 1 mM KCl and 2 mM MgATP, the distance trajectory showed fast fluctuations between 4 to 5 nm (Figure 2B). This is in good agreement with the distance between the selected labeling positions in the modeled structures of KdpB in the closed (4 nm) and open state (5 nm) (Figure 1A).
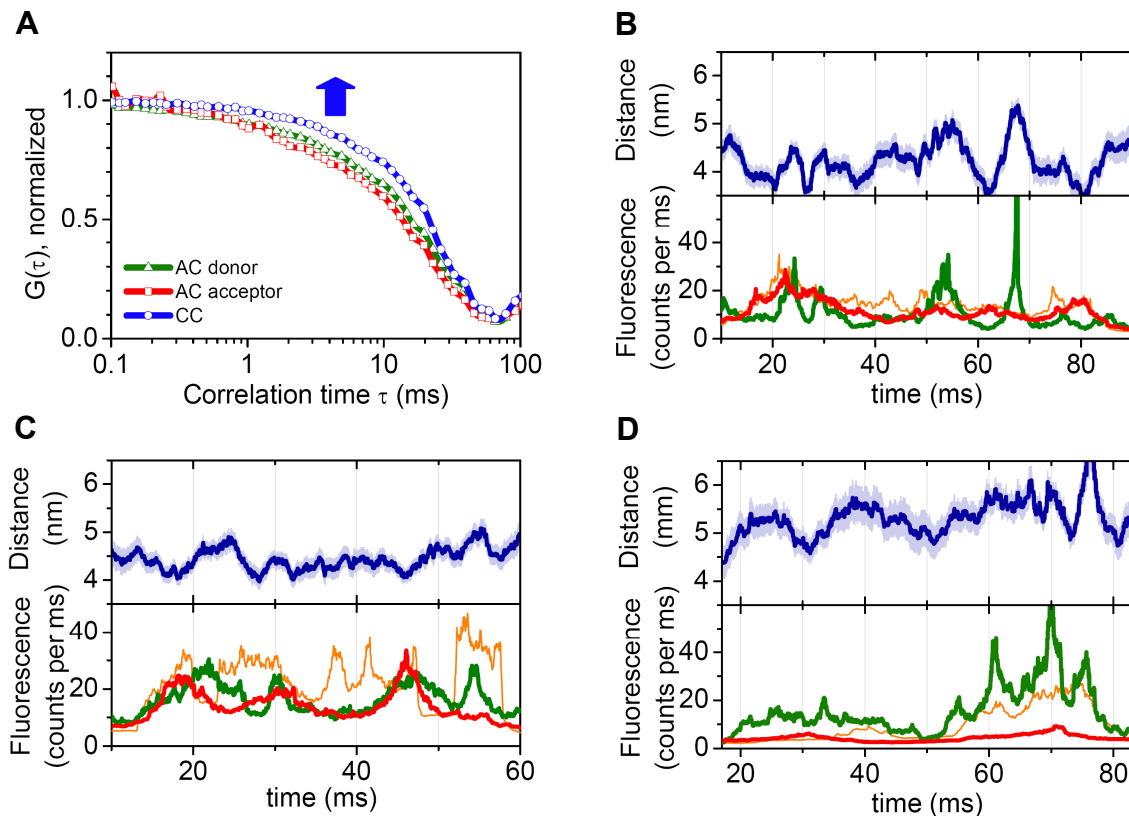

Figure 2. Single-molecule FRET data of reconstituted KdpFABC. (A) Fluorescence autocorrelation functions for FRET-labeled KdpFABC during catalysis. FRET donor (green curve) and acceptor (red curve) exhibit the same diffusion time of about 16 ms, whereas the cross-correlation (blue curve) of FRET donor and acceptor shows the characteristic deviation (blue arrow) due to FRET state transitions with a time constant of about 3.5 ms. (B-D), FRET-induced photon bursts of single KdpFABC complexes. The lower panels show fluorescence intensity traces of FRET donor (green trace) and FRET acceptor (red trace) excited with 488 nm as well as FRET acceptor intensities excited with 635 nm (orange trace). Time traces are shown as moving average of 50 photons for each detection channel. Corresponding distance trajectories (blue traces with standard deviation in light blue) between the labels bound to the N- and the A-domain are shown in the upper panels. (B) Catalysis in the presence of 1 mM KCl and 2 mM ATP. (C) As B, plus inhibitor 200 µM *ortho*-vanadate. (D) As B, plus inhibitor 500 µM OCS.

In order to trap one conformation, 200 µM *ortho*-vanadate was added (Figure 2C), which is assumed to block the enzyme in the closed E2-P state (*3, 38-40*). Surprisingly, both distances still occurred but the dwell times of these states were elongated. To large extent, the same results were obtained with 500 µM OCS, which is reported to block Na$^+$,K$^+$- ATPase presumably in the E1 state (*41*). However, in case of OCS, the distances were slightly enlarged and mainly ranged between 5 to 6 nm (Figure 2D).

Dwell times of fast fluctuating states in the millisecond time scale can be estimated using fluorescence correlation methods. We selected a set of 33 KdpFABC complexes apparently switching between several interdomain distances in the presence of ATP and KCl and calculated the normalized autocorrelation functions of the FRET donor and of the FRET acceptor intensities as well as the corresponding cross correlation function (Figure 2A). Conformational dynamics of the N- and A-domain were expected to result in anti-correlated FRET donor and acceptor intensities. For the autocorrelation function, this causes an additional decay term with a specific time constant and, simultaneously, a rise term in the cross correlation function. The deviation in the cross correlation function was associated with a time constant of about 3.5 ms, which indicated a fast dwell time for one particular conformation in KdpFABC complexes.

In order to discriminate between specific conformational states, especially in the case of rather small dwell times, a Hidden-Markov-Model (HMM) approach (42-47) was elaborated based on the FRET efficiency trajectories from the 1 ms time-binned intensity data. A three-state HMM (Supplemental, Figure VI) has recently been successfully used to analyze single molecule FRET data of the rotary motions of subunits in F_OF_1-ATP synthase (48). Here, the HMM was further refined to overcome the problems of FRET state turning points within one time bin (49). These time bins occur with a rather high frequency and could lead to an assignment of a hidden state to an averaged observable. However, state transitions are indicated by a reduced corresponding likelihood value of the Markov chain for those time bins. So far, we used the summed number of FRET donor and acceptor photons per time bin as a weighting key for the accuracy of the measured proximity factor. Now, including the reduced likelihood value at the transition points as weighting key diminished the contribution of time bins with a high probability of an inherent state transition. A series of models ranging from 2 to 10 hidden states were trained on the data set, which resulted in a most-likely description of the KdpFABC dynamics by three independent conformations called S1 (~5 nm), S2 (~4 nm) and S3 (~6 nm). Examples of state assignments in individual transporters are shown in Figure 3A-C. The S1 states were consistent with the distances of the open conformation (E1; ~5 nm), and the S2 states were related to the distances of the closed conformation (~4 nm), which corresponds to the biochemical states E1~P, E2-P and E2. The population of a wide-open S3 state with a short dwell time of 3 ms was small and transitions to S3 only occurred infrequently. Among the three biochemical conditions tested (catalysis, *ortho*-vanadate and OCS inhibition), the overall distribution of states did not change significantly (S1: 38 %, S2: 49 % and S3: 13 %). To gain more information about the predominant order of transitions between these three states, two-dimensional FRET transition density plots according to ref (43) were created (Figure 3D-F). Again, a similar distribution of transitions was found in all three cases, with dominating transitions between S1 and S2. Furthermore, the S3 state only shifted to the S1 state and *vice versa*, but never to the S2 state.
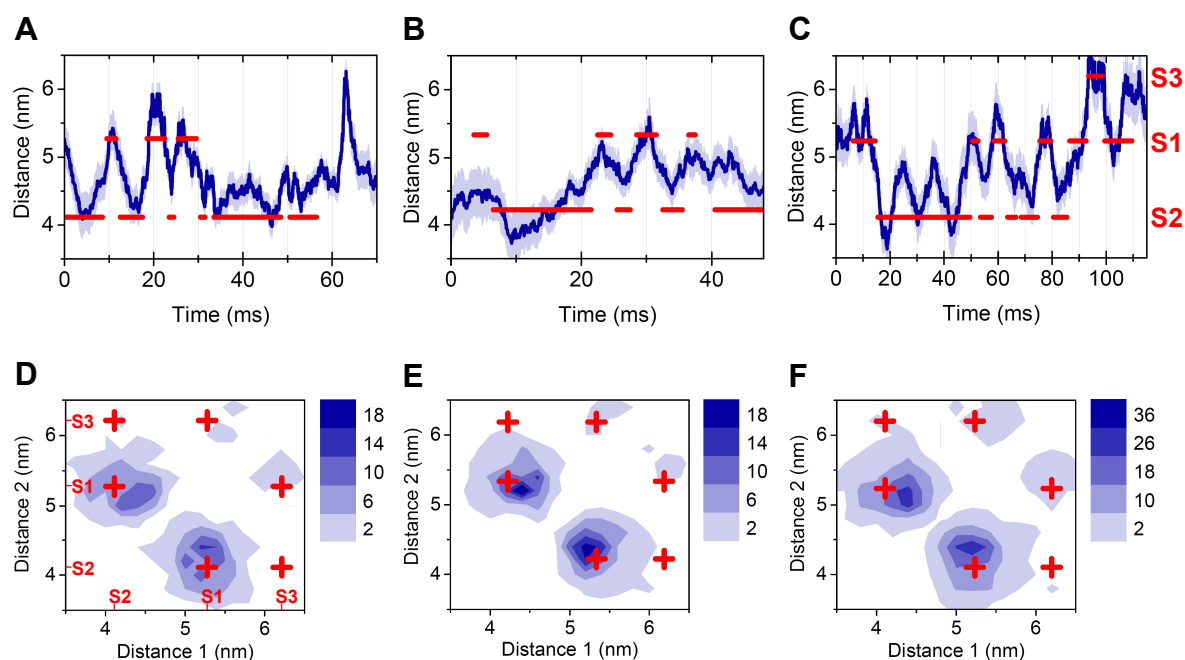
Figure 3: FRET level transition analysis based on Hidden-Markov-Models (HMM). (A-C) FRET distance changes in labeled KdpFABC during catalysis without (A) and upon addition of 200 µM *ortho*-vanadate (B) or 500 µM OCS (C). Red lines indicate the learned S1 (~5 nm), S2 (~4 nm) and S3 (~6 nm) HMM states and the dwell according to the HMM. (D-F) FRET transition density plots for the HMM-assigned states. For better understanding, the three states are highlighted in red on the distance axes of D. Red crosses mark the six possible state transitions; blue contours show the distribution of the actual FRET distances for each state. For all biochemical conditions, two similar dominating transitions were found, i.e. between the S1 and the S2 state. The low-FRET S3 state is only populated from and shifts to S1.

In order to determine the dwell times of the three states and to check whether the presence of an S3 state might be an artifact from short-term arbitrarily co-localized fluorescent impurities, the FRET data sets were re-analyzed manually. First, switching points between constant FRET levels in single KdpFABC complexes were assigned. FRET efficiencies and resultant real distances were calculated for each FRET level based on the fluorescence intensities [I] of both FRET donor and acceptor and, independently, on the lifetimes [τ] of the FRET donor. The consistence of FRET distance determination is shown in the two-dimensional plots (Figure 4A-C). This plot was also used for quality control of the analyzed data. Detected FRET levels have to result in the same distances independently of which mode of calculation was used. As a consequence, the datapoints have to be arranged close by the red lines in Figures 4A-C. Subsequently, FRET levels were sorted with respect to the expected FRET distance intervals for the S1 state (between 4.7 and 5.3 nm), the S2 state (between 3.5 and 4.7 nm) and the S3 state (>5.3nm). The frequency of the S3 state was too low for further dwell time analysis. Using these limits, the dwell time distribution for the S1 and the S2 state was plotted for every biochemical condition (Figure 4D-F). The corresponding curve fittings are shown as lines together with the dwell times calculated. In the presence of 1 mM KCl and 2 mM MgATP, the dwell time of the closed conformation (S2) was 7.5 ms and for the open

(S1) conformation 3.9 ms. Assuming a full transport cycle going from S1 to S2 to S1, the sum of both dwell times corresponds to turnover rates of 80 to 100 s^{-1} at room temperature. This is in the same range as the turnover rates of other P-type ATPases like SERCA (100 s^{-1}) (*50*) or Na^{+},K^{+}-ATPase (30-50 s^{-1}) (*51*). *Ortho*-vanadate prolonged the open S1 state (~19 ms), whereas, in the presence of OCS, both dwell times were prolonged (S1: ~24 ms, S2: ~17 ms).
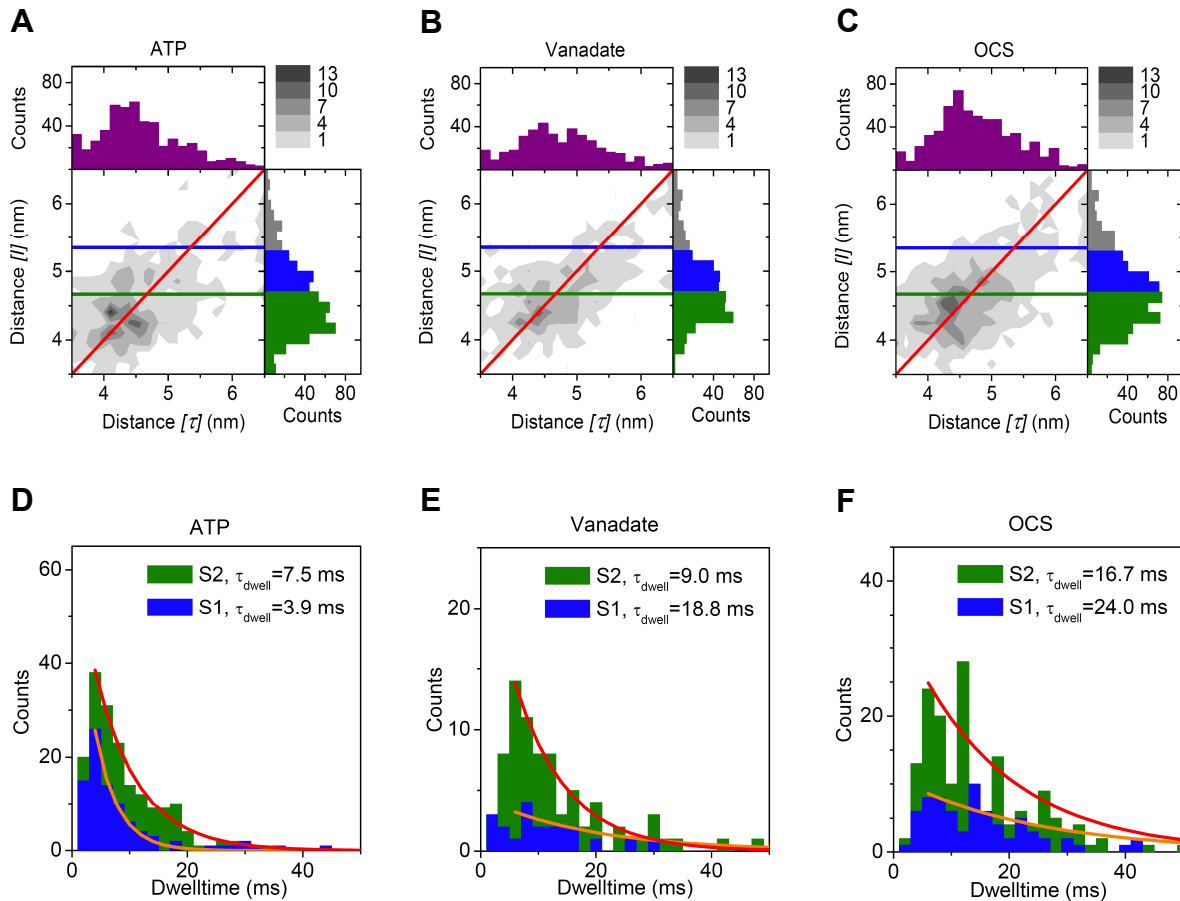

Figure 4: Manual assignment of KdpB conformations and dwell times. (A-C) Distributions of distances between the N- and the A-domain as calculated from FRET based on intensities [*I*] versus FRET based on donor lifetimes [τ] for reconstituted KdpFABC during catalysis. The closed conformation of KdpFABC (S2 state) is assigned to distances < 4.7 nm, the open conformation to distances between 4.7 nm and 5.3 nm. (D-F) Corresponding dwell time distributions for the S1 and S2 states. In the presence of the inhibitors *ortho*-vanadate or OCS, both dwell times are significantly prolonged.

DISCUSSION

Since the late 50's when Skou linked ion transport to ATPase activity by discovering the Na^+,K^+-ATPase (*52*), P-type ATPases are under intensive investigations. Today, huge information is available regarding the structure of P-type ATPases locked in different catalytic states. Furthermore, there is already a detailed view of the putative reaction cycle of P-type ATPases primarily based on biochemical data. One of the most important features of P-type ATPases is the large domain movements during the catalytic cycle. However, up to date, these domain movements have either been shown freezed in crystal structures under non-native conditions or only indirectly during catalysis via modulation of the intrinsic tryptophan fluorescence or digestion experiments (For overview: *23-27*). Furthermore, especially crystal structures share no information about how frequent and how long the crystallized conformation appears in the catalytic cycle. Therefore, direct and detailed data about the dynamics of the structural changes are still missing.

We have used the single molecule ALEX-FRET technique to monitor the dynamics of single molecules of the P-type ATPase KdpFABC from *E. coli* in real-time, both under ATP hydrolyzing as well as under inhibiting conditions. The use of small fluorescent maleimides for labeling instead of rather large fluorescent fusion proteins like GFP together with the reconstitution of the protein complexes into liposomes minimizes any artificial effects on protein dynamics by providing native conditions as far as possible. The FRET measurements demonstrated the presence of primarily two distinct states, S1 and S2, which appeared at an equal frequency. The calculated distances of these states of approximately 5 nm (S1) and 4 nm (S2) are in well accord with the predicted distances of the labeling positions in KdpB for the E1 and E2 state as derived from homology modelling by use of SERCA crystal structures. However, the distance states (S1 and S2) differ from the biochemical states (E1, E2) in a way that the phosphorylated E1~P and E2-P state also belong to the S2 distance (Figure 5). In the vast majority of cases, the S1 state shifts to the S2 state and *vice versa*, which strongly reflects the proposed reaction cycle. An additional third state (S3) could also be observed, which corresponded to a rather large distance of approximately 6 nm. However, this conformational state could not be described by the reaction cycle of KdpFABC or any other P-type ATPase. In fact, the low frequency of this state indicated that it plays no role in the reaction cycle. Furthermore, the S3 state only originates from and shifts to the S1 state but was never related to S2. The N-domain of P-type ATPases is thought to be linked to the P-domain by two flexible linker regions (*3*) and undergoes large tilting movements during ATP-hydrolysis. Therefore, it is likely that in the open S1 state, the N-domain tilts back and forth from the A-domain due to thermal fluctuations, thus casually forming the wide open S3 state (Figure 5).

Although several catalytic substeps have been resolved by structural analysis especially in the case of SERCA (*3-6, 8-10*), these structures yielded no information about the flexibility of the P-type ATPase domains in these states. In this work, we could clearly show that the different distance states correlating with the biochemical states fluctuated at high frequency. Even inhibiting conditions did not notably affect the flexibility of the enzyme. *Ortho*-vanadate was shown to block the Na^+,K^+-ATPase biochemically in the E2-P state by tightly binding at the conserved aspartate residue in the P-domain, thereby blocking the dephosphorylation (*38-40*). The fitting of the TNP-AMP-bound E1 state crystal structure of SERCA into the SERCA electron density map of the vanadate-bound E2-P state (*3*) identified a large spherical mass at the P-domain near the conserved aspartate residue, which most likely represents a decavanadate molecule. An additional binding of the inhibitor to the N-domain has never been shown. Our results favour the notion that the vanadate molecule indeed binds to the P-domain but does not interact with the N-domain. This could result in a conformational state, in which the enzyme is biochemically blocked by the vanadate molecule without affecting the flexibility of the N-domain. Therefore, the N-domain is still free to swing back and forth resulting in the two distance states S1 and S2. However, the rather large vanadate molecule could constrict the N-domain just a bit, thereby resulting in elongated dwell times of the structural states, especially of the large-distance S1 state (4.8x). The more recently described inhibitor OCS was shown to biochemically block the Na^+,K^+-ATPase in the E1 state by binding to the cytoplasmic side of the protein (*41*) and also inhibits SERCA (*53*) and the KdpFABC complex (data not shown). Our results demonstrate that also OCS does not block the enzyme in a particular distance state (S1 or S2). Incubation with OCS rather resulted in significantly prolonged dwell times especially of the S1 state (S1: 6x, S2: 2.2x) but did not prevent the shift into the S2 state. This could be explained by a binding of OCS at a position, which blocks the enzyme biochemically in the E1 state and, in addition, somewhat effects the N- and A-domain flexibility.
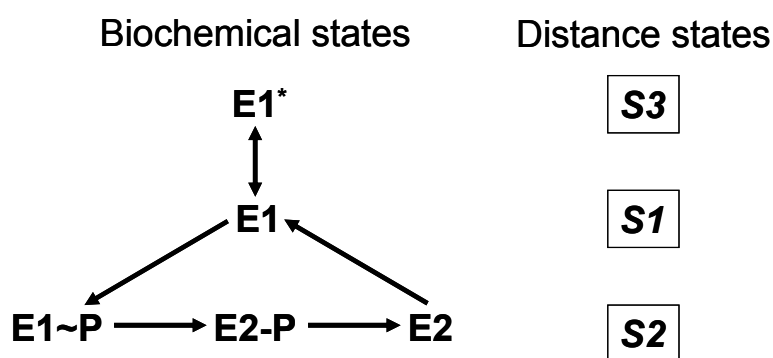

Figure 5: Assignment of the proposed biochemical states [E] to the identified distance states [S]. The KdpFABC complex is proposed to undergo the typical E1/E2 reaction cycle of P-type ATPases. The biochemical E1 state is consistent with the measured open conformation S1. The closed conformation S2 involves the biochemical states E1~P, E2-P and E2. During the reaction cycle (indicated by arrows), S1 shifts to S2 and *vice versa*. The rare wide-open conformation S3 only exchanges with S1 and could be explained by occasional short-lived back-tilting of the flexible N-domain. This state is most likely not involved in the reaction cycle as indicated by the E1* state.

The analysis of dwell times during catalysis indicated that the S2 state is the rate-limiting step of the P-type reaction cycle. As depicted in Figure 5, the S2 state involves the three enzymatic states E1~P, E2-P and E2, whereas the S1 state corresponds to only the E1 state. As a consequence, the S2 state involves a higher number of catalytic substeps. However, the E2/E1 transition was identified as the rate-limiting step in Na^+,K^+-ATPase (*54*). In the case of SERCA, the rate-limiting step of the reaction cycle is supposed to be related to the E1~P/E2-P transition (*55*). Both of these results structurally correspond to the S2 state in our case and, thus, are well in accord with our data. By use of single molecule ALEX-FRET, we directly measured distance changes within KdpB during ATP hydrolysis, which is the first time that such single molecule real-time dynamic measurements were made for P-type ATPases. Resolving both the distance changes and the according dwell times for three conformational states under catalysis as well as in the *ortho*-vanadate- and the OCS-inhibited state, this technique provides new insights into the functional dynamics of the KdpFABC complex and P-type ATPases in general.

ACKNOWLEDGMENT

SUPPLEMENTAL
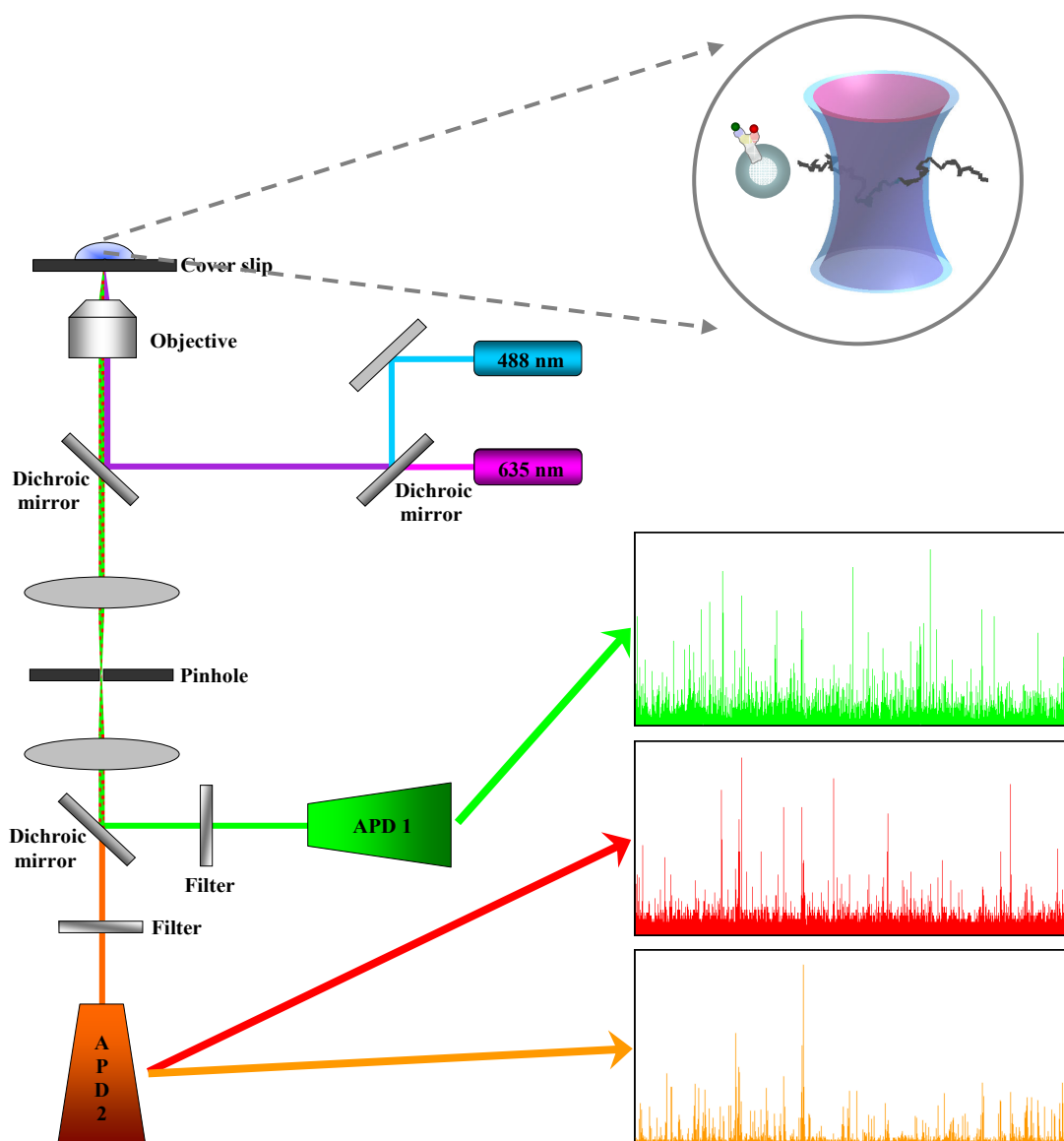
Figure I: Alternating laser excitation microscopic setup. The donor excitation laser at 488 nm and the acceptor excitation laser at 635 nm emit laser pulses in an alternating fashion. By use of a dichroic mirror, both lasers were overlaid and thereupon directed into the microscope objective by a second dichroic mirror. The objective focuses both laser beams into the sample, resulting in a confocal volume of a few femtoliters. Fluorophores diffusing through the confocal volume emit light of a lower wavelength as the excitation lasers, which is collected by the objective and passes the dichroic mirror. Subsequently, a lens focuses the fluorescence light beam, which allows for passage through a 150 µm pinhole. This pinhole defines the confocal detection volume and prevents light scattering toward the extremely sensitive avalanche photodiodes (APD). Beyond the pinhole, the fluorescent light beam is again widened by a second lens. The following dichroic mirror separates the donor fluorescence from the acceptor fluorescence. After passing a correspondingly selective filter, the fluorescence is detected by an avalanche photo diode.
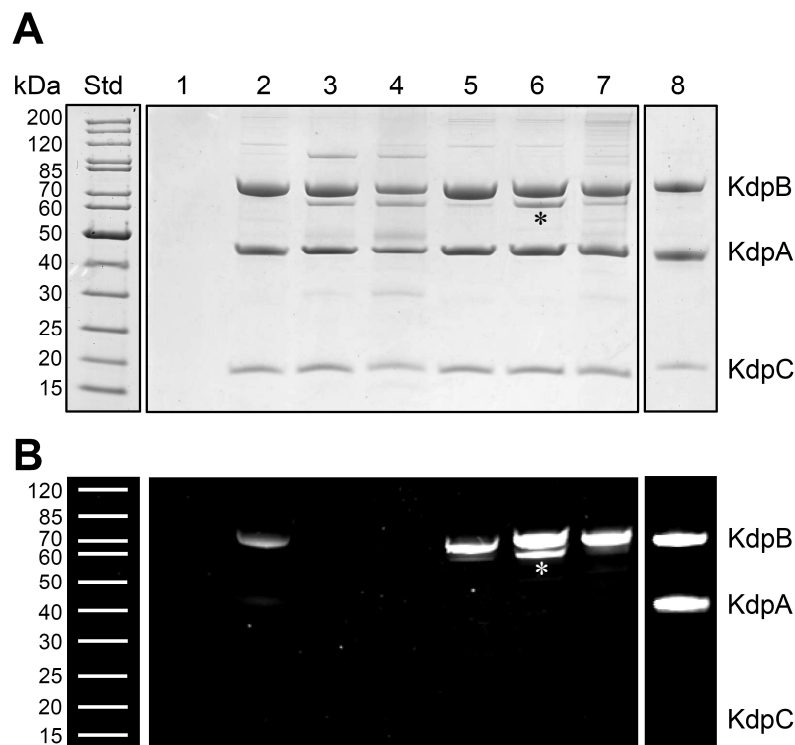
Figure II: Protection of the membrane-integral cysteine residues in liposomes and labeling specificity of the introduced cysteines. Isolated KdpFABC, KdpFABCΔCys (KdpFABC complexes, in which all cysteine residues have been replaced), and KdpFABCΔCys with different cysteine substitutions were reconstituted into liposomes at a protein/lipid ratio of 1:20 followed by labeling of 5 μg of protein with Alexa 488-maleimide in a complex/dye ratio of 1:40. Subsequently, labeled proteoliposomes were subjected to SDS-PAGE. Proteins were either stained with Coomassie (A) or visualized by exposition on a UV transilluminator (B). Std, molecular-mass standard; 1, plain control liposomes; 2, KdpFABC wild type; 3, KdpFABCΔCys; 4, KdpFABCΔCys-KdpB:A261C/A609C; 5, KdpFABCΔCys-KdpB:A261C/A609C/G150C; 6, KdpFABCΔCys-KdpB:A261C/A609C/A407C; 7 KdpFABCΔCys-KdpB:A261C/A609C/G150C/A407C; 8, KdpFABC wild type denatured with 1 % (w/v) SDS prior to the addition of the fluorophore. A degradation product of KdpB is marked with asterisks. Explanations for the mutants are given in the text and in Appendix, Table 2. Only the introduced cysteines in the A- and N-domain (G150C and A407C, respectively) could be labeled. The membrane-integral cysteines of KdpB (C261 and C609) are completely prevented from labeling. Furthermore, unspecific labeling of the cysteine-free KdpA and KdpC subunit does not occur.
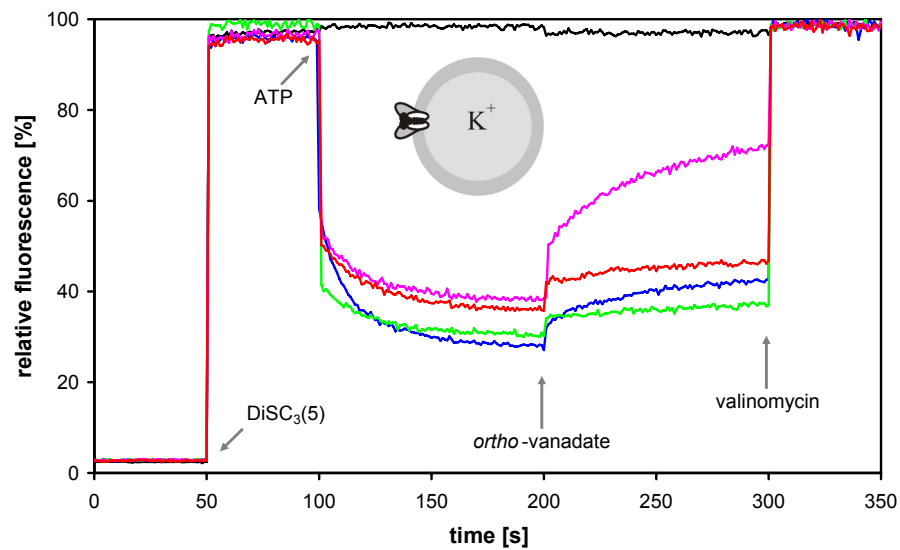
Figure III: Electrogenic K⁺ transport of reconstituted wild type and mutant KdpFABC complexes. Fluorometric measurements were carried out in the presence of 50 mM KCl inside and outside of the proteoliposomes. The ATP-driven export of K⁺ by inside-out reconstituted KdpFABC complexes was initiated by the addition of 1 mM ATP at the time indicated. The translocation of K⁺ imposes a membrane potential, which is readily detected by the potential-sensitive fluorophore $DiSC_3(5)$. Specific inhibition of transport activity by the addition of *ortho*-vanadate served as a control for active transport by the P-type ATPase, whereas the final addition of valinomycin served as a control of K⁺ specificity of the signal. Four different fluorescence traces are shown: black, plain control liposomes; blue, KdpFABC wild type; green, KdpFABCΔCys-KdpB:A261C/A609C/G150C; magenta, KdpFABCΔCys-KdpB:A261C/A609C/A407C; red, KdpFABCΔCys-KdpB:A261C/A609C/G150C/A407C. Explanations for the mutants are given in the text and in Appendix, Table 2. All mutant KdpFABC complexes show almost identical potassium transport kinetics as the wild type complex.
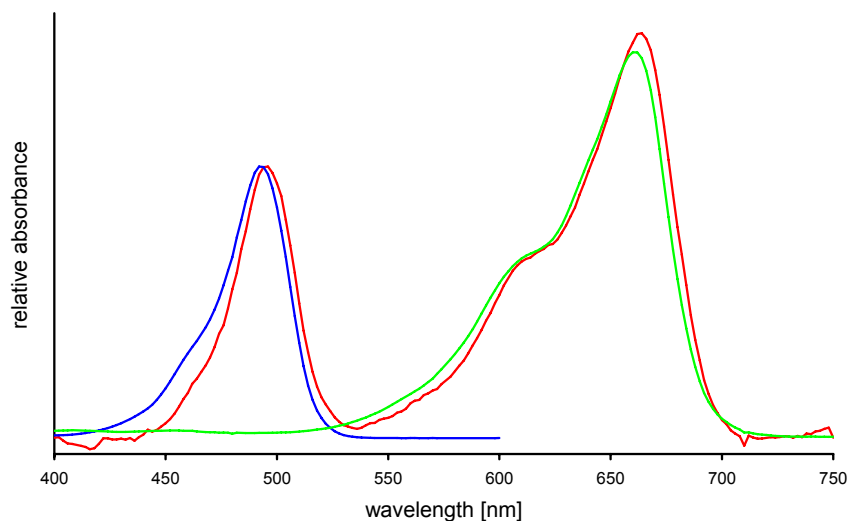
Figure IV: Absorption spectra of reconstituted KdpFABC complexes labeled with Alexa 488- and ATTO 655-maleimide. KdpFABCΔCys-KdpB:A261C/A609C/G150C/A407C was reconstituted into liposomes at a protein/lipid ratio of 1:20 followed by labeling of the proteoliposomes as described previously. After solubilization with 1 % Triton-X-100, absorbance spectra were measured and corrected by subtracting buffer absorbance spectra. The absorbance spectrum of the labeled KdpFABC-mutant (red) is almost identical to the spectra of the free Alexa 488-maleimide (blue) and ATTO 655-maleimide (green).
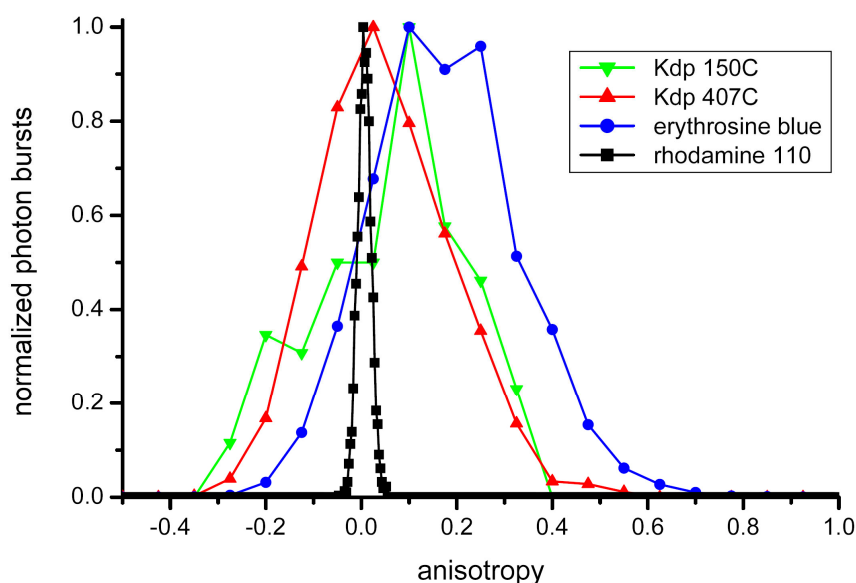
Figure V: Single-molecule fluorescence anisotropy plots. KdpFABC complexes carrying either the G150C (KdpFABCΔCys-KdpB:A261C/A609C/G150C; green) or A407C substitution (KdpFABCΔCys-KdpB:A261C/A609C/G150C/A407C; red) were labeled with Alexa 488-maleimide as described. Fluorescence anisotropy was measured on a modified single-molecule FRET setup. The free dye rhodamine 110 (black) was used as a reference without anisotropy and erythrosine blue (blue) as positive anisotropy reference. Only the G150C substitution shows a slight, however negligible anisotropy.
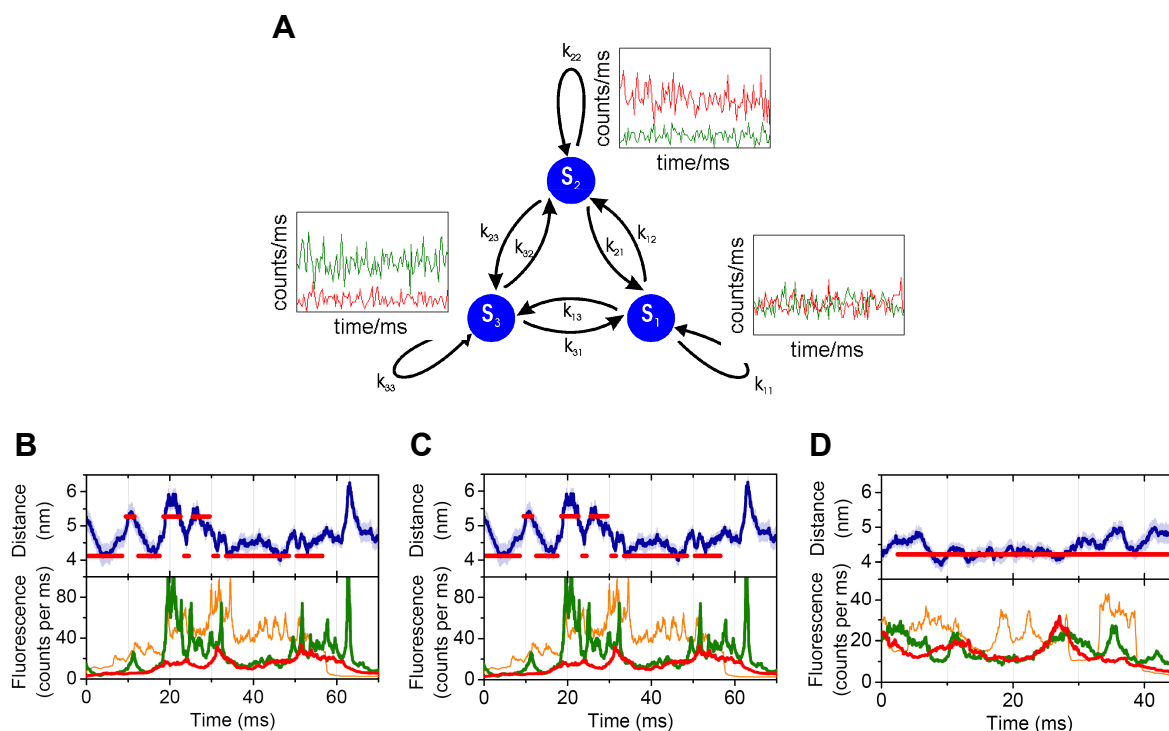
Figure VI: Three-state Hidden-Markov-Model (HMM). (A) HMM with possible transitions applied to the FRET level search within the selected FRET-induced KdpFABC photon bursts. The S1 state was assigned to represent a medium FRET efficiency state, S2 was a high FRET efficiency state and S3 was a low FRET efficiency state. S3 was attributed to approx. 6 nm (13 % of all assigned states), S1 corresponded to approx. 5 nm (38 % of all assigned states), and S2 was found at approx. 4 nm (49 % of all assigned states). (B-D) FRET distance changes in selected bursts found by a three-state HMM during catalysis without (B) and with 200 µM *ortho*-vanadate (C) or 500 µM OCS (D).

REFERENCES

1. Møller, J. V., Juul, B., and le Maire, M. (1996) Structural organization, ion transport, and energy transduction of P-type ATPases. *Biochim. Biophys. Acta 1286*, 1-51.

2. Axelsen, K. B., and Palmgreen, M. G. (1998) Evolution of substrate specificities in the P-type ATPase superfamily. *J. Mol. Evol. 46*, 84-101.

3. Toyoshima, C., Nakasako, M., Nomura, H., and Ogawa, H. (2000) Crystal structure of the calcium pump of sarcoplasmic reticulum at 2.6 Å resolution. *Nature 405*, 647-655.

4. Toyoshima, C., and Nomura, H. (2002) Structural changes in the calcium pump accompanying the dissociation of calcium. *Nature 418*, 605-611.

5. Toyoshima, C., Nomura, H., and Sugita, Y. (2003) Crystal structures of Ca^{2+}-ATPase in various physiological states. *Ann. N.Y. Acad. Sci. 986*, 1-8.

6. Toyoshima, C., and Mizutani, T. (2004) Crystal structure of the calcium pump with a bound ATP analogue. *Nature 430*, 529- 535.

7. Olesen, C., Sørensen, T. L., Nielsen, R. C., Møller, J. V., and Nissen, P. (2004) Dephosphorylation of the calcium pump coupled to counterion occlusion. *Science 306*, 2251-2255.

8. Olesen, C., Picard, M., Winther, A.-M., Gyrup C., Morth, J. P., Oxvig, C., Møller, J. V., and Nissen, P. (2007) The structural basis of calcium transport by the calcium pump. *Nature 450*, 1036-1042.

9. Rice, W. J., Young, H. S., Martin, D. W., Sachs, J. R., and Stokes, D. L. (2001) Structure of the Na^+,K^+-ATPase at 11 Å resolution: comparison with Ca^{2+}-ATPase in E1 and E2 states. *Biophys. J. 80*, 2187–2197.

10. Morth, J. P., Pedersen, B. P., Toustrup-Jensen, M. S., Sørensen, T. L., Petersen, J., Andersen, J. P., Vilsen, B., and Nissen, P. (2007) Crystal structure of the sodium-potassium pump. *Nature 450*, 1043-1049.

11. Pedersen, P. L., and Carafoli, E. (1987) Ion motive ATPases. I. Ubiquity, properties, and significance to cell function. *Trends Biochem. Sci. 12*, 146-150.

12. Bertrand, J., Altendorf, K., and Bramkamp, M. (2004) Amino acid substitutions in putative selectivity filter regions III and IV in KdpA alter ion selectivity of the KdpFABC complex from *Escherichia coli*. *J. Bacteriol. 186*, 5519-5522.

13. Buurman, E. T., Kim, K. T., and Epstein, W. (1995) Genetic evidence for two sequentially occupied K^+ binding sites in the Kdp transport ATPase. *J. Biol. Chem. 270*, 6678-6685.

14. Schrader, M., Fendler, K., Bamberg, E., Gaßel, M., Epstein, W., Altendorf, K., and Dröse, S. (2000) Replacement of glycine 232 by aspartic acid in the KdpA subunit broadens the ion specificity of the K^+-translocating KdpFABC complex. *Biophys. J. 79*, 802-813.

15. van der Laan, M., Gaßel, M., and Altendorf, K. (2002) Characterization of amino acid substitutions in KdpA, the K^+-binding and -translocating subunit of the KdpFABC complex of *Escherichia coli*. *J. Bacteriol. 184*, 5491-5494.

16. Durell, S. R., Bakker, E. P., and Guy, H. R. (2000) Does the KdpA subunit from the high affinity K^+-translocating P-type Kdp-ATPase have a structure similar to that of K^+ channels? *Biophys. J. 77*, 775-788.

17. Bramkamp, M., and Altendorf, K. (2005) Single amino acid substitution in the putative transmembrane helix V in KdpB of the KdpFABC complex of *Escherichia coli* uncouples ATPase activity and ion transport. *Biochemistry 44*, 8260-8266.

18. Gaßel, M., and Altendorf, K. (2001) Analysis of KdpC of the K^+-transporting KdpFABC complex of *Escherichia coli*. *Eur. J. Biochem. 268*, 1772-1781.

19. Ahnert, F., Schmid, R., Altendorf, K., and Greie, J.-C. (2006) ATP binding properties of the soluble part of the KdpC subunit from the *Escherichia coli* K^+-transporting KdpFABC P-type ATPase. *Biochemistry 45*, 11038-11046.

20. Gaßel, M., Möllenkamp, T., Puppe, W., and Altendorf, K. (1999) The KdpF subunit is part of the K^+-translocating Kdp complex of *Escherichia coli* and is responsible for stabilization of the complex *in vitro*. *J. Biol. Chem. 274*, 37901-37907.

21. Post, R. L., Hegyvary, C., and Kume, S. (1972) Activation by adenosine triphosphate in the phosphorylation kinetics of sodium and potassium ion transport adenosine triphosphatase. *J. Biol. Chem. 247*, 6530-6540.

22. Albers, R. W. (1967) Biochemical aspects of active transport. *Annu. Rev. Biochem. 36*, 727-756.

23. Kubala, M. (2006) ATP-binding to P-type ATPases as revealed by biochemical, spectroscopic, and crystallographic experiments. *Proteins 64*, 1-12.

24. Horisberger, J. D. (2004) Recent insights into the structure and mechanism of the sodium pump. *Physiology 19*, 377-387.

25. Kanazawa, T., Suzuki, H., Daiho, T., and Yamasaki, K. (1995) Fluorometric study on conformational changes in the catalytic cycle of sarcoplasmic reticulum Ca^{2+}-ATPase. *Biosci. Rep. 15*, 317-326.

26. Karlish, S. J., Goldshleger, R., Tal, D. M., Capasso, J. M., Hoving, S., and Stein, W. D. (1992) Identification of the cation binding domain of Na^+,K^+-ATPase. *Acta. Physiol. Scand. Suppl. 607*, 69-76.

27. Shin, J. M., Besancon, M., Bamberg, K., and Sachs, G. (1997) Structural aspects of the gastric H^+,K^+-ATPase. *Ann. N. Y. Acad. Sci. 834*, 65-76.

28. Heitkamp, T., Kalinowski, R., Böttcher, B., Börsch, M., Altendorf, K., and Greie, J-C. (2008) K^+-translocating KdpFABC P-Type ATPase from *Escherichia coli* acts as a functional and structural dimer. *Biochemistry 47*, 3564–3575.

29. Henkel, R. D., Van De Berg, J. L., and Walsh, R. A. (1988) A microassay for ATPase. *Anal. Biochem. 169*, 312-318.

30. Altendorf, K., Gaßel, M., Puppe, W., Möllenkamp, T., Zeeck, A., Boddien, C., Fendler, K., Bamberg, E., and Dröse, S. (1998) Structure and function of the Kdp-ATPase of *Escherichia coli*. *Acta Physiol. Scand. 163*, 137-146

31. Fendler, K., Dröse, S., Altendorf, K., and Bamberg, E. (1996) Electrogenic K^+ transport by the Kdp-ATPase of *Escherichia coli*. *Biochemistry 35*, 8009-8017.

32. Zimmermann, B., Diez, M., Zarrabi, N., Gräber, P., and Börsch, M. (2005) Movements of the ε-subunit during catalysis and activation in single membrane-bound H^+-ATP synthase. *EMBO J. 24*, 2053-2063.

33. Börsch, M., Diez, M., Zimmermann, B., Reuter, R., and Gräber, P. (2002) Stepwise rotation of the γ-subunit of EF_oF_1 ATP synthase observed by intramolecular single-molecule fluorescence resonance energy transfer. *FEBS lett. 527*, 147-152.

34. Börsch, M., and Gräber, P. (2005) Subunit movement in individual H^+-ATP synthases during ATP synthesis and hydrolysis revealed by fluorescence resonance energy transfer. *Biochem. Soc. Trans. 33*, 878-882.

35. Zimmermann, B., Diez, M., Börsch, M., and Gräber, P. (2006) Subunit movements in membrane-integrated EF_oF_1 during ATP synthesis detected by single-molecule spectroscopy. *BBA-Bioenergetics 1757*, 311-319.

36. Förster, T. (1948) Zwischenmolekulare Energiewanderung und Fluoreszenz. *Ann. Phys. 2*, 55-70.

37. Sørensen, T. L., Møller, J. V., and Nissen, P. (2004) Phosphoryl transfer and calcium ion occlusion in the calcium pump. *Science 304*, 1672-1675.

38. Cantley, L. C. Jr., Cantley, L. G., and Josephson, L. (1978) A characterization of vanadate interactions with the Na^+,K^+-ATPase. Mechanistic and regulatory implications. *J. Biol. Chem. 253*, 7361-7368.

39. Karlish, S. J., Beaugé, L. A., and Glynn, I. M. (1979) Vanadate inhibits Na^+,K^+-ATPase by blocking a conformational change of the unphosphorylated form. *Nature 282*, 333-335.

40. Smith, R. L., Zinn, K., and Cantley, L. C. (1980) A study of the vanadate-trapped state of the (Na^+,K^+)-ATPase. Evidence against interacting nucleotide site models. *J. Biol. Chem. 255*, 9852-9859.

41. Stimac, R., Kerek, F., and Apell, H. J. (2005) Mechanism of the Na^+,K^+-ATPase inhibition by MCS derivatives. *J. Membr. Biol. 205*, 89-101.

42. Murphy, K. P. (2001) Computing Science and Statistics 33.

43. McKinney, S. A., Joo, C., and Ha, T. (2006) Analysis of single-molecule FRET trajectories using hidden Markov modeling. *Biophys. J. 91*, 1941-1951.

44. Viterbi, A. J. (1967) Error Bounds for Convolutional Codes and an Asymptotically Optimum Decoding Algorithm. *Ieee Transactions on Information Theory It13*, 260-269.

45. Baum, L. E., Petrie, T., Soules, G., and Weiss, N. (1970) A Maximization Technique Occurring in Statistical Analysis of Probabilistic Functions of Markov Chains. *Ann. Math. Stat. 41*, 164-171.

46. Hastie, R. T. T., and Friedman, J. (2001) The Elements of Statistical Learning: Data Mining, Inference, and Prediction. *Springer-Verlag*, New York.

47. Talaga, D. (2007) Markov processes in single molecule fluorescence. *Curr. Opin. Colloid. In. 12*, 285-296.

48. Zarrabi, N., Düser, M. G., Ernst, S., Reuter, R., Glick, G. D., Dunn, S. D., Wrachtrup, J., and Börsch, M. (2007) Monitoring the rotary motors of single F_oF_1-ATP synthase by synchronized multi channel TCSPC. *Proc. SPIE 6771*, 67710F.

49. Zarrabi, N., Heitkamp, T., Greie, J.-C., and Börsch, M. (2008) Monitoring the conformational dynamics of a single potassium transporter by ALEX-FRET. *Proc. SPIE 6862*, 68620M.

50. Sørensen, T. L., Clausen, J. D., Jensen, A. M., Vilsen, B., Møller, J. V., Andersen, J. P., and Nissen, P. (2004) Localization of a K^+-binding site involved in dephosphorylation of the sarcoplasmic reticulum Ca^{2+}-ATPase. *J. Biol. Chem. 279*, 46355-46358.

51. Costa, C. J., Gatto, G., and Kaplan, J. H. (2003) Interactions between Na^+,K^+-ATPase α-Subunit ATP-binding Domains. *J. Biol. Chem. 278*, 9176-9184.

52. Skou, J. C. (1957) The Influence of Some Cations on an Adenosine Triphosphatase from Peripheral Nerves. *Biochim. Biophys. Acta 23*, 394-401.

53. Kerek, F., Stimac, R., Apell, H. J., Freudenmann, F., and Moroder, L. (2002) Characterization of the macrocyclic carbon suboxide factors as potent Na^+,K^+-ATPase and SR Ca^{2+}-ATPase inhibitors. *Biochim. Biophys. Acta 1567*, 213-220.

54. Lüpfert, C., Grell, E., Pintschovius, V., Apell, H. J., Cornelius, F., and Clarke, R. J. (2001) Rate Limitation of the Na^+,K^+-ATPase Pump Cycle. *Biophys. J. 81*, 2069-2081.

55. Champeil, P., le Maire, M., Andersen, J. P., Guillain, F., Gingold, M., Lund, S., and Møller, J. V. (1986) Kinetic characterization of the normal and detergent-perturbed reaction cycles of the sarcoplasmic reticulum calcium pump. Rate-limiting step(s) under different conditions. *J. Biol. Chem. 261*, 16372-16384.

NOTE

In this chapter a three state Hidden-Markov-Model as well as several MATLAB-based scripts for the computational analysis of the single-molecule ALEX-FRET data were used, which were elaborated by Nawid Zarrabi during his Ph.D. thesis.

Furthermore, plasmids encoding cysteine-free *kdpA* and *kdpB* mutants were kindly provided by Doris Becker. In this study, these plasmids were used to generate the pGS4ΔCys plasmid for the production of a KdpFABC complex lacking all cysteines.

Finally, homology modeling of KdpB was carried out by Henrik Strahl. In the present chapter, the corresponding pdb-file was used to generate Figure 1A.

SUMMARY

The bacterial KdpFABC complex adopts an exceptional position in the field of P-type ATPases. It exhibits some unique features, which are not found in any other P-type ATPase and which are mainly reflected by its unique subunit composition. This applies especially to the spatial separation of ion transport (mediated by KdpA) and ATP hydrolysis (mediated by KdpB) as well as to the putative cooperative interaction of the N-domain of KdpB and the C-terminal part of KdpC. Studies on the KdpFABC complex from *Escherichia coli* so far concentrated mainly on the similarities of KdpA to KcsA-like potassium channels, on the energy coupling between KdpB and KdpA, on the biochemical features of KdpB and KdpA and on the structure of the nucleotide binding domain of KdpB. The elucidation of the macromolecular structure of the complex has so far almost been neglected. However, the knowledge just on the arrangement of subunits could provide new insights into the interplay of the single components. Therefore, two chapters of this thesis focus on the determination of the low resolution structure of the KdpFABC complex. Whereas the first chapter elucidates the native oligomeric state of KdpFABC, the second chapter provides a low resolution structural map of the monomeric enzyme complex.

Although the KdpFABC complex exhibits some unique features among P-type ATPases, it also shares other common features of this ATPase family, especially with respect to the large domain movements during the characteristic reaction cycle. However, these dynamic domain movements have never been directly shown for any P-type ATPase. For the first time, chapter three provides direct experimental data on the dynamics of domain distance changes and corresponding dwell times of the two major catalytical states in the functionally active enzyme.

The oligomeric state of the KdpFABC complex has been determined by multiple techniques. Chemical cross-linking of native cysteines in KdpB by use of copper 1,10-phenanthroline resulted in the formation of a high molecular weight cross-link product, which could be identified as a KdpB dimer and demonstrated the presence of neighboring KdpB subunits. The cysteine residues responsible for cross-linking were identified by mutagenesis as C48 and C679, both of which are located near the periplasmic side of the protein. Gel filtration analysis of cross-linked KdpFABC together with non-cross-linked complexes resulted in only one single peak at an apparent molecular weight corresponding to a homodimer, which indicated that KdpFABC had already been purified as a dimer. In order to directly analyze KdpFABC dimers, negatively stained enzyme complexes were visualized by transmission electron microscopy, demonstrating a nearly 1:1 distribution of monomeric and dimeric KdpFABC complexes. These results suggest a concentration-dependent dissociation of the complex due to the high dilution (20-50 nM) used for electron microscopic

specimen preparation. Finally, functionally reconstituted KdpFABC complexes were analyzed by single molecule FRET in freely diffusing liposomes. For this purpose, KdpFABC preparations were site-directedly reacted with sulfhydryl-specific derivatives of ATTO 488 and ATTO 655 at just one position in KdpB prior to reconstitution, resulting in a heterogeneously labeled enzyme preparation. As a result, FRET could only occur in the case of dimeric KdpFABC complexes. The data obtained further restricted the dissociation constant of the monomer/dimer equilibrium to 30-50 nM, which is consistent with the dissociation constants of other dimeric P-type ATPases. These data have already been published (Heitkamp *et al.*, 2008)

In order to obtain more detailed information about the subunit arrangement within the enzyme complex, negatively stained KdpFABC was further analyzed by single particle transmission electron microscopy. Analysis of approximately 10,000 monomeric complexes resulted in an electron density map corresponding to a solution structure at a resolution of 19 Å. In contrast to previous electron tomographic data obtained with 2D crystal lattices of KdpFABC, the model presented in this thesis also contains distinct information on the large membrane-embedded part of the complex. Three-dimensional structural homology models of the single subunits could be fitted into the map, which allowed for conclusions about subunit interfaces. The K^+-translocating KdpA subunit is in tight contact with the transmembrane domain of the ATP-hydrolyzing KdpB subunit. Because of the essential energy coupling between KdpA and KdpB, this contact has already been predicted. Furthermore, the cytosolic C-terminal portion of KdpC could be located in close vicinity to the N-domain of KdpB, thereby allowing a direct interaction during the assumed cooperative ATP binding mechanism. Furthermore, the electron density map was used to build a docking model of two KdpFABC complexes based on the information obtained from the analyses of the oligomeric state. This docking model brings the P-domains of the KdpB subunits in close vicinity to each other and shows a tight cogging of the monomers. These data have already been submitted for publication in the Journal of Structural Biology, the corresponding manuscript is under revision.

P-type ATPases exhibit a typical reaction cycle with several biochemically and structurally different substeps. However, two major conformations can be distinguished, which mainly result from large movements of the N- and A-domain. So far, most information on these conformations was obtained from crystal structures of eukaryotic P-type ATPases, which have been trapped in several catalytical substeps. Nevertheless, these domain movements of P-type ATPases have so far never been shown directly in the catalytically active enzyme.
In this thesis, distance changes between the N- and the A-domain of catalytically active KdpFABC could be observed directly and, thus, for the first time for a P-type ATPase. This was achieved by measuring single molecule FRET on freely diffusing proteoliposomes by use of an alternating laser

excitation scheme (ALEX). Isolated KdpFABC complexes were site-specifically labeled with sulfhydryl-specific Alexa 488- and ATTO 655-derivatives at both the N- and the A-domain of KdpB and subsequently reconstituted in liposomes. Single molecule FRET was measured under ATP-hydrolyzing conditions as well as in the vanadate- and OCS- inhibited states. Manual analysis of the resulting datasets as well as an automated Hidden-Markov approach resulted in three distinct distance states for every biochemical condition, namely S1 (~5 nm), S2 (~4 nm) and S3 (~6 nm). The S1 and the S2 states are well in accord with the expected distances in the open (E1) and the closed (E2) conformation of KdpB. Under catalytic conditions, dwell times of 3.9 ms (S1) and 7.5 ms (S2) could be determined, which in sum correlated well with the general catalytic turnover number of P-type ATPases. However, the observed S2 state could be identified as the rate limiting step of the reaction cycle, which is further consistent with biochemical data of other P-type ATPases. Furthermore, inhibition of the complex by vanadate or OCS did not result in locking the flexible domains into a single rather rigid conformation. In terms of catalysis, inhibition rather resulted in an elongation of the dwell times of both states. The rare S3 state was populated from and transited only to the S1 state, thereby indicating a structural conformation, which is not relevant for the reaction cycle and eventually merely results from the high flexibility of the N-domain. These data are subject to publication.

APPENDIX

Table 1: Primer used in this study

name	sequence	purpose
KdpA-C64A-for	CAATATCTT<u>GCT</u>GCCATTCTCGGCCTGAAC	KdpA: Substitution C64A
KdpA-C64A-rev	CAGGCCGAGAATGGC<u>AGC</u>AAGATATTGCTT	KdpA: Substitution C64A
KdpA-C267A-for	CCAACGGCGCTGG<u>GCC</u>TTTGCCTTTGGTGAA	KdpA: Substitution C267A
KdpA-C267A-rev	ACCAAAGGCAAA<u>GGC</u>CAGCGCCGTTGGGAT	KdpA: Substitution C267A
KdpA-C294A-for	ATTTTTGTCATC<u>GCC</u>GTAGGCGTGGTGATG	KdpA: Substitution C294A
KdpA-C294A-rev	CATCACCACGCCTAC<u>GGC</u>GATGACAAAAAT	KdpA: Substitution C294A
KdpA-C344S-for	GCGGCTTCC<u>TCT</u>GGCGCGGTGATTGCGATGCATGATTCGTTT	KdpA: Substitution C344S
KdpA-C344S-rev	AAACGAATCATGCATCGCAATCACCGCGCC<u>AGA</u>GGAAGCCGC	KdpA: Substitution C344S
KdpA-C483AC488A-for	TCTCCGTTCTGGAAC<u>GCT</u>TTACTGGCGTTC<u>GCC</u>ATGTTTGTCGGTCGC	KdpA: Substitution C483A and C488A
KdpA-C483AC488A-rev	GCGACCGACAAACAT<u>GGC</u>GAACGCCAGTAA<u>AGC</u>GTTCCAGAACGGAGA	KdpA: Substitution C483A and C488A
KdpA-EcoRI-for	CAGCCA**GAATTC**TACCCTTCCGGTAT	KdpA: Substitution C64A
KdpA-NcoI-for	CAGCTGTTAC**CCATGG**GGCCTGTAGCT	KdpA: Substitution C267A,C294A and C344S
KdpA-NcoI-rev	AGCTACAGGCC**CCATGG**GTAACAGCTG	KdpA: Substitution C64A
KdpA-NsiI-for	GTGATTGCG**ATGCAT**GATTCGTTTACC	KdpA: Substitution C483A and C488A
KdpA-NsiI-rev	CGAATC**ATGCAT**CGCAATCACCGCGCCACAGGAAGC	KdpA: Substitution C267A and C294A
KdpA-BsiWI-rev	TTCATCTCG**CGTACG**TCGATTTTTTTA	KdpA: Substitution C344S
KdpA-BstBI-rev	AAGTGTTGG**TTCGAA**TAGCGCCAGTTG	KdpA: Substitution C483A and C488A

Substitutions of amino acid residues are underlined. Recognition sequences for restriction endonucleases are highlighted in bold type.

Table 1: Primer used in this study

name	sequence	purpose
KdpB-C48A-for	GCTGACCACC<u>GCT</u>ATTAGCATCG	KdpB: Substitution C48A
KdpB-C48A-rev	CGATGCTAAT<u>AGC</u>GGTGGTCAGC	KdpB: Substitution C48A
KdpB-C142S-for	GATATTATCCCC<u>TCC</u>GATGGTGAAGTT	KdpB: Substitution C142S
KdpB-C142S-rev	AACTTCACCATC<u>GGA</u>GGGGATAATATC	KdpB: Substitution C142S
KdpB-C191S-HpaI-rev	CTCGCCGGG**GTTAAC**GCT<u>AGA</u>CTCAATCACCAG	KdpB: Substitution C48A, C142S and C191S
KdpB-C261A-for	GCGCTGCTGGTC<u>GCT</u>CTGATCCCAACC	KdpB: Substitution C261A
KdpB-C261A-rev	GGTTGGGATCAG<u>AGC</u>GACCAGCAGCGC	KdpB: Substitution C261A
KdpB-C609A-for	CTGAACATCATG<u>GCC</u>CTGCATTCGCCC	KdpB: Substitution C609A
KdpB-C609A-rev	GGGCGAATGCAG<u>GGC</u>CATGATGTTCAG	KdpB: Substitution C609A
KdpB-C679A-for	CTGCTGACCGTT<u>GCC</u>GGTCTGGTGTG	KdpB: Substitution C679A
KdpB-C679A-rev	CACACCAGACC<u>GGC</u>AACGGTCAGCAG	KdpB: Substitution C679A
KdpB-MfeI-for	GTGATGG**CAATTG**CCGGTTCGC	KdpB: Substitution C48A, C142S and C191S
KdpB-HpaI-for	TGTAGC**GTTAAC**CCCGGCGAG	KdpB: Substitution C261A
KdpB-ClaI-rev	CATGCGGTT**ATCGAT**GTTGATC	KdpB: Substitution C261A
KdpB-BamHI-for	GACCCGT**GGATCC**CTGACCACCTTCAG	KdpB: Substitution C609A and C679A
KdpB-SalI-rev	TAAAT**GTCGAC**AATGCCGGAC	KdpB: Substitution C609A and C679A
KdpB-A407C-Up-for	GTGATCCTCGCCAAGCAGCG	KdpB: Substitution A407C
KdpB-A407C-Up-rev	CCACCGTTACACTCAACATGGCG	KdpB: Substitution A407C
KdpB-A407C-Down-for	CGCCATGTTGAGTGTAACGGTGG	KdpB: Substitution A407C
KdpB-A407C-Down-rev	CACCGCACTGAGGATTGCGG	KdpB: Substitution A407C
KdpB-G150C-Up-for	GCCTTTGCCGGCTTAAGCGC	KdpB: Substitution G150C
KdpB-G150C-Up-rev	CGACCGATGCACACCCTTC	KdpB: Substitution G150C
KdpB-G150C-Down-for	GAAGGGTGTGCATCGGTCG	KdpB: Substitution G150C
KdpB-G150C-Down-rev	GGCACTCGCTGACAACAGGC	KdpB: Substitution G150C

Substitutions of amino acid residues are underlined. Recognition sequences for restriction endonucleases are highlighted in bold type.

Table 2: Plasmids used in this study

name	genotype	characteristics	resulting protein
pGS4	Ap^R, P_{kdp}, $kdpFA_{His}BC$	expression of $kdpFA_{His}BC$	KdpFABC
pGS4-KdpB(C48A)	Ap^R, P_{kdp}, $kdpFA_{His}BC$, $kdpB^{C48A}$	expression of $kdpFA_{His}BC$; substitution C48A within KdpB	KdpFAB(C48A)C
pGS4-KdpB(C679A)	Ap^R, P_{kdp}, $kdpFA_{His}BC$, $kdpB^{C679A}$	expression of $kdpFA_{His}BC$, substitution C679A within KdpB	KdpFAB(C679A)C
pGS4ΔCys	Ap^R, P_{kdp}, $kdpFA_{His}BC$, $kdpA^{C(64, 267, 294, 483, 488)A, C344S}$, $kdpB^{C(48, 261, 609, 679)A, C(142, 191)S}$	expression of $kdpFA_{His}BC$; substitution of all cysteines within KdpFABC	KdpFABCΔCys
pGS4ΔCys-KdpB(C261)	Ap^R, P_{kdp}, $kdpFA_{His}BC$, $kdpA^{C(64, 267, 294, 483, 488)A, C344S}$, $kdpB^{C(48, 609, 679)A, C(142, 191)S}$	expression of $kdpFA_{His}BC$; substitution of all cysteines within KdpFABC, except C261 of KdpB	KdpFABCΔCys-KdpB:A261C
pGS4ΔCys-KdpB(C609)	Ap^R, P_{kdp}, $kdpFA_{His}BC$, $kdpA^{C(64, 267, 294, 483, 488)A, C344S}$, $kdpB^{C(48, 261, 679)A, C(142, 191)S}$	expression of $kdpFA_{His}BC$; substitution of all cysteines within KdpFABC, except C261 and C609 of KdpB	KdpFABCΔCys-KdpB:A609C
pGS4ΔCys-KdpB(C261/C609)	Ap^R, P_{kdp}, $kdpFA_{His}BC$, $kdpA^{C(64, 267, 294, 483, 488)A, C344S}$, $kdpB^{C(48, 679)A, C(142, 191)S}$	expression of $kdpFA_{His}BC$; substitution of all cysteines within the KdpFABC complex, except C261 and C609 of KdpB	KdpFABCΔCys-KdpB:A261C/A609C
pGS4ΔCys-KdpB(C261/C609/G150C)	Ap^R, P_{kdp}, $kdpFA_{His}BC$, $kdpA^{C(64, 267, 294, 483, 488)A, C344S}$, $kdpB^{C(48, 679)A, C(142, 191)S, G150C}$	expression of $kdpFA_{His}BC$; substitution of all cysteines within the KdpFABC complex, except C261 and C609 of KdpB; substitution G150C within KdpB	KdpFABCΔCys-KdpB:A261C/A609C/G150C
pGS4ΔCys-KdpB(C261/C609/A407C)	Ap^R, P_{kdp}, $kdpFA_{His}BC$, $kdpA^{C(64, 267, 294, 483, 488)A, C344S}$, $kdpB^{C(48, 679)A, C(142, 191)S, A150C}$	expression of $kdpFA_{His}BC$; substitution of all cysteines within the KdpFABC complex, except C261 and C609 of KdpB; substitution A407C within KdpB	KdpFABCΔCys-KdpB:A261C/A609C/A407C
pGS4ΔCys-KdpB(C261/C609/G150C/A407C)	Ap^R, P_{kdp}, $kdpFA_{His}BC$, $kdpA^{C(64, 267, 294, 483, 488)A, C344S}$, $kdpB^{C(48, 679)A, C(142, 191)S, G150C, A407C}$	expression of $kdpFA_{His}BC$; substitution of all cysteines within the KdpFABC complex, except C261 and C609 of KdpB; substitution G150C and A407C within KdpB	KdpFABCΔCys-KdpB:A261C/A609C/G150C/A407C

The plasmid pGS4 is taken from Ahnert *et al.* (2006). The plasmids pGS4-KdpB(C48A) and pGS4-KdpB(C679A) were made by René Kalinowski during his diploma thesis.

CURRICULUM VITAE

Personal Information

Name: Thomas Heitkamp

Date/Place of Birth: 11.04.1979, Osnabrück (Germany)

Citizenship: German

Marital Status: Single

Education

Since 07/2004	**Doctoral thesis in biological science**

Doctoral thesis in biological science

Universität Osnabrück, Fachbereich Biologie/Chemie

Arbeitsgruppe Mikrobiologie (SFB 431)

PhD thesis: „Structure and functional dynamics of the KdpFABC P-type ATPase from *Escherichia coli*.“

05/2004   **Diploma in biological science**

Universität Osnabrück, Fachbereich Biologie/Chemie

Arbeitsgruppe Mikrobiologie

Diploma thesis: „Untersuchung zur Struktur und Funktion der regulatorischen Usp-Domäne aus den kdp-Operonen von *Halobacterium salinarum* und *Escherichia coli*.“

10/1998 – 05/2004   **Studies in biology**

Universität Osnabrück

08/1991 – 06/1998   **General qualification for university entrance (Abitur)**

Gymnasium Bad Essen, Germany

Erklärung über die Eigenständigkeit der erbrachten wissenschaftlichen Leistung

Ich erkläre hiermit, dass ich die vorliegende Arbeit ohne unzulässige Hilfe Dritter und ohne Benutzung anderer als der angegebenen Hilfsmittel angefertigt habe. Die aus anderen Quellen direkt oder indirekt übernommenen Daten und Konzepte sind unter Angabe der Quelle gekennzeichnet.

Bei der Auswahl und Auswertung folgenden Materials haben mir die nachstehend aufgeführten Personen in der jeweils beschriebenen Weise unentgeltlich geholfen.

1. Die Cystein-cross-link Experimente erfolgten in Zusammenarbeit mit René Kalinowski (Abteilung Mikrobiologie, Fachbereich Biologie/Chemie, Universität Osnabrück) und wurden von mir reproduziert und vertieft.

2. Die Modellierung der Strukturen von KdpA, KdpB und $KdpC_{90-188}$ erfolgte von Henrik Strahl (Abteilung Mikrobiologie, Fachbereich Biologie/Chemie, Universität Osnabrück).

3. Die Konstruktion der Cystein-freien KdpA- und KdpB-Plasmide erfolgte von Doris Becker (Abteilung Mikrobiologie, Fachbereich Biologie/Chemie, Universität Osnabrück)

4. Die Entwicklung des 3-Stufen Hidden-Markov-Modells erfolgte von Nawid Zarrabi innerhalb der Kooperation mit der Arbeitsgruppe von Dr. Michael Börsch (3. Physikalisches Institut, Universität Stuttgart).

Weitere Personen waren an der inhaltlichen materiellen Erstellung der vorliegenden Arbeit nicht beteiligt. Insbesondere habe ich hierfür nicht die entgeltliche Hilfe von Vermittlungs- bzw. Beratungsdiensten (Promotionsberater oder andere Personen) in Anspruch genommen. Niemand hat von mir unmittelbar geldwerte Leistungen für Arbeiten erhalten, die im Zusammenhang mit dem Inhalt der vorgelegten Dissertation stehen.

Die Arbeit wurde bisher weder im In- noch im Ausland in gleicher oder ähnlicher Form einer anderen Prüfungsbehörde vorgelegt.

---------------------------------   ---------------------------------

       (Ort, Datum)   (Unterschrift)